



1 Systematic Characterization and Fluorescence Threshold Strategies for the Wideband Integrated
2 Bioaerosol Sensor (WIBS) Using Size-Resolved Biological and Interfering Particles

3 NICOLE SAVAGE¹, Christine Krentz¹, Tobias Könemann², Taewon T. Han³, Gediminas
4 Mainelis³, Christopher Pöhlker², John A. Huffman¹

5 ¹ *University of Denver, Department of Chemistry and Biochemistry, Denver, USA*

6 ² *Max Planck Institute for Chemistry, Multiphase Chemistry and Biogeochemistry Departments,
7 Mainz, Germany*

8 ³ *Rutgers, The State University of New Jersey, Department of Environmental Science, New
9 Jersey, USA*

10

11 **Abstract**

12 Atmospheric particles of biological origin, also referred to as bioaerosols or primary biological
13 aerosol particles (PBAP), are important to various human health and environmental systems.
14 There has been a recent steep increase in the frequency of published studies utilizing commercial
15 instrumentation based on ultraviolet laser/light-induced fluorescence (UV-LIF), such as the
16 WIBS (wideband integrated bioaerosol sensor) or UV-APS (ultraviolet aerodynamic particle
17 sizer), for bioaerosol detection both outdoors and in the built environment. Significant work over
18 several decades supported the development of the general technologies, but efforts to
19 systematically characterize the operation of new commercial sensors has remained lacking.
20 Specifically, there have been gaps in the understanding of how different classes of biological and
21 non-biological particles can influence the detection ability of LIF-instrumentation. Here we
22 present a systematic characterization of the WIBS-4A instrument using 69 types of aerosol
23 materials, including a representative list of pollen, fungal spores, and bacteria as well as the most
24 important groups of non-biological materials reported to exhibit interfering fluorescent
25 properties. Broad separation can be seen between the biological and non-biological particles
26 directly using the five WIBS output parameters and by taking advantage of the particle
27 classification analysis introduced by Perring et al. (2015). We highlight the importance that
28 particle size plays on observed fluorescence properties and thus in the Perring-style particle
29 classification. We also discuss several particle analysis strategies, including the commonly used
30 fluorescence threshold defined as the mean instrument background (forced trigger; FT) plus 3
31 standard deviations (σ) of the measurement. Changing the particle fluorescence threshold was
32 shown to have a significant impact on fluorescence fraction and particle type classification. We
33 conclude that raising the fluorescence threshold from FT + 3 σ to FT + 9 σ does little to reduce the
34 relative fraction of biological material considered fluorescent, but can significantly reduce the
35 interference from mineral dust and other non-biological aerosols. We discuss examples of highly
36 fluorescent interfering particles, such as brown carbon, diesel soot, and cotton fibers, and how
37 these may impact WIBS analysis and data interpretation in various indoor and outdoor
38 environments. A comprehensive online supplement is provided, which includes size distributions
39 broken down by fluorescent particle type for all 69 aerosol materials and comparing two
40 threshold strategies. Lastly, the study was designed to propose analysis strategies that may be
41 useful to the broader community of UV-LIF instrumentation users in order to promote deeper



42 discussions about how best to continue improving UV-LIF instrumentation and analysis
43 strategies.

44 1. Introduction

45 Biological material emitted into the atmosphere from biogenic sources on terrestrial and
46 marine surfaces can play important roles in the health of many living systems and may influence
47 diverse environmental processes (Cox and Wathes, 1995;Pöschl, 2005;Després et al.,
48 2012;Fröhlich -Nowoisky et al., 2016). Bioaerosol exposure has been an increasingly important
49 component of recent interest, motivated by studies linking airborne biological agents and adverse
50 health effects in both indoor and occupational environments (Douwes et al., 2003). Bioaerosols
51 may also impact the environment by acting as giant cloud condensation nuclei (GCCN) or ice
52 nuclei (IN), having an effect on cloud formation and precipitation (Ariya et al., 2009;Delort et
53 al., 2010;Möhler et al., 2007;Morris et al., 2004). Biological material emitted into the
54 atmosphere is commonly referred to as Primary Biological Aerosol Particles (PBAP) or
55 bioaerosols. PBAP can include whole microorganisms, such as bacteria and viruses, reproductive
56 entities (fungal spores and pollen) and small fragments of any larger biological material, such as
57 leaves, vegetative detritus, fungal hyphae, or biopolymers, and can represent living, dead,
58 dormant, pathogenic, allergenic, or biologically inert material (Després et al., 2012). PBAP often
59 represent a large fraction of supermicron aerosol, for example up to 65% by mass in pristine
60 tropical forests, and may also be present in high enough concentrations at submicron sizes to
61 influence aerosol properties (Jaenicke, 2005;Penner, 1994;Pöschl et al., 2010).

62 Until recently the understanding of physical and chemical processes involving bioaerosols
63 has been limited due to a lack of instrumentation capable of characterizing particles with
64 sufficient time and size resolution (Huffman and Santarpia, 2017). The majority of bioaerosol
65 analysis historically utilized microscopy or cultivation-based techniques. Both are time-
66 consuming, relatively costly and cannot be utilized for real-time analysis (Griffiths and
67 Decosemo, 1994;Agranovski et al., 2004). Cultivation techniques can provide information about
68 properties of the culturable fraction of the aerosol (e.g. bacterial and fungal spores), but can
69 greatly underestimate the diversity and abundance of bioaerosols because the vast majority of
70 microorganism species are not culturable (Amann et al., 1995;Chi and Li, 2007;Heidelberg et al.,
71 1997). Further, because culture-based methods cannot detect non-viable bioaerosols, information
72 about their chemical properties and allergenicity has been poorly understood.

73 In recent years, advancements in the chemical and physical detection of bioaerosols have
74 enabled the development of rapid and cost-effective techniques for the real-time characterization
75 and quantification of airborne biological particles (Ho, 2002;Hairston et al., 1997;Huffman and
76 Santarpia, 2017;Sodeau and O'Connor, 2016). One important technique is based on ultraviolet
77 laser/light-induced fluorescence (UV-LIF), originally developed by military research
78 communities for the rapid detection of bio-warfare agents (BWA) (e.g. Hill et al., 2001;Hill et
79 al., 1999a;Pinnick et al., 1995). More recently, UV-LIF instrumentation has been
80 commercialized for application toward civilian research in fields related to atmospheric and
81 exposure science. The two most commonly applied commercial UV-LIF bioaerosol sensors are
82 the wideband integrated bioaerosol sensor (WIBS; University of Hertfordshire, Hertfordshire,
83 UK, now licensed to Droplet Measurement Technologies, Longmont, CO, USA), and the
84 ultraviolet aerodynamic particle sizer (UV-APS; licensed to TSI, Shoreview, MN, USA). Both



85 sensors utilize pulsed ultraviolet light to excite fluorescence from individual particles in a real-
86 time system. The wavelengths of excitation and emission were originally chosen to detect
87 biological fluorophores assumed to be widely present in airborne microorganisms (e.g.
88 tryptophan-containing proteins, NAD(P)H co-enzymes, or riboflavin) (Pöhlker et al., 2012).
89 Significant work was done by military groups to optimize pre-commercial sensor performance
90 toward the goal of alerting for the presence of biological warfare agents such as anthrax spores.
91 The primary objective from this perspective is to positively identify BWAs without being
92 distracted by false-positive signals from fluorescent particles in the surrounding natural
93 environment (Primmerman, 2000). From the perspective of basic atmospheric science, however,
94 the measurement goal is often to quantify bioaerosol concentrations in a given environment. So,
95 to a coarse level of discrimination, BWA-detection communities aim to ignore most of what the
96 atmospheric science community seeks to detect. Researchers on such military-funded teams also
97 have often not been able to publish their work in formats openly accessible to civilian
98 researchers, so scientific literature is lean on information that can help UV-LIF users operate and
99 interpret their results effectively. Early UV-LIF bioaerosol instruments have been in use for two
100 decades and commercial instruments built on similar concepts are emerging and becoming
101 widely used by scientists in many disciplines. In some cases, however, papers are published with
102 minimal consideration of complexities of the UV-LIF data. This study presents a detailed
103 discussion of several important variables specific to WIBS data interpretation, but that can apply
104 broadly to operation and analysis of many similar UV-LIF instruments.

105 The commercially available WIBS instrument has become one of the most commonly
106 applied instrument toward the detection and characterization of bioaerosol particles in both
107 outdoor and indoor environments. As will be discussed in more detail, the instrument utilizes two
108 wavelengths of excitation (280 nm and 370 nm), the second of which is close to the one
109 wavelength utilized by the UV-APS (355 nm). Both the WIBS and UV-APS, in various version
110 updates, have been applied to many types of studies regarding outdoor aerosol characterization.
111 For example they have been important instruments: in the study of ice nuclei (Huffman et al.,
112 2013; Mason et al., 2015; Twohy et al., 2016), toward the understanding of outdoor fungal spore
113 concentrations (Gosselin et al., 2016; Saari et al., 2015a; O'Connor et al., 2015b), to investigate
114 the concentration and properties of bioaerosols from long-range transport (Hallar et al., 2011), in
115 tropical aerosol (Gabey et al., 2010; Whitehead et al., 2010; Huffman et al., 2012; Valsan et al.,
116 2016; Whitehead et al., 2016), in urban aerosol (Huffman et al., 2010; Saari et al., 2015b; Yu et al.,
117 2016), from composting centers (O'Connor et al., 2015), at high altitude (Crawford et al.,
118 2016; Gabey et al., 2013; Perring et al., 2015; Ziemba et al., 2016), and in many other
119 environments (Healy et al., 2014; Li et al., 2016; O'Connor et al., 2015a). The same
120 instrumentation has been utilized for a number of studies involving the built, or indoor,
121 environment as well (Wu et al., 2016). As a limited set of examples, these instruments have been
122 critical components in the study of bioaerosols in the hospital environment (Lavoie et al.,
123 2015; Handorean et al., 2015) and to study the emission rates of biological particles directly from
124 humans (Bhangar et al., 2016) in school classrooms (Bhangar et al., 2014), and in offices (Xie et
125 al., 2017).

126 Despite the numerous and continually growing list of studies that utilize commercial UV-LIF
127 instrumentation, only a handful of studies have published results from laboratory work
128 characterizing the operation or analysis of the instruments in detail. For example, Kananni et al.
129 (2007, 2008, 2009) and Agranovski et al. (2003, 2004, 2005) presented several examples of UV-



130 APS operation with respect to bio-fluorophores and biological particles. Healy et al. (2012)
131 provided an overview of fifteen spore and pollen species analyzed by the WIBS, and Toprak and
132 Schnaiter (2013) discussed the separation of dust from ambient fluorescent aerosol by applying a
133 simple screen of any particles that exhibited fluorescence in one specific fluorescent channel.
134 Hernandez et al. (2016) presented a summary of more than 50 pure cultures of bacteria, fungal
135 spores, and pollen species analyzed by the WIBS and with respect to fluorescent particle type.
136 Fluorescent particles observed in the atmosphere have frequently been used as a lower-limit
137 proxy for biological particles (e.g. Huffman et al. 2010), however it is well known that a number
138 of key particle types of non-biological origin can fluoresce. For example, certain examples of
139 soot, humic and fulvic acids, mineral dusts, and aged organic aerosols can exhibit fluorescent
140 properties, and the effects that these play in the interpretation of WIBS data is unclear (Bones et
141 al., 2010; Gabey et al., 2011; Lee et al., 2013; Pöhlker et al., 2012; Sivaprakasam et al., 2004).

142 The simplest level of analysis of WIBS data is to provide the number of particles that exceed
143 the minimum detectable threshold in each of the three fluorescence categories. Many papers on
144 ambient particle observations have been written using this data analysis strategy with both the
145 WIBS and UV-APS data. Such analyses are useful and can provide an important first layer of
146 discrimination by fluorescence. To provide more complicated discrimination as a function of
147 observed fluorescence intensity, however, brings associated analysis and computing challenges,
148 i.e. users often must write data analysis code themselves and processing large data sets can push
149 the limits of standard laboratory computers. Discriminating based on fluorescence intensity also
150 requires more detailed investigations into the strategy by which fluorescent thresholds can be
151 applied to define whether a particle is considered fluorescent. Additionally, relatively little
152 attention has been given to the optical properties of non-biological particles interrogated by the
153 WIBS and to optimize how best to systematically discriminate between biological aerosol of
154 interest and materials interfering with those measurements.

155 Here we present a comprehensive and systematic laboratory study of WIBS data in order to
156 aid the operation and data interpretation of commercially available UV-LIF instrumentation. This
157 work presents 69 types of aerosol materials, including key biological and non-biological
158 particles, interrogated by the WIBS-4A and shows the relationship of fluorescent intensity and
159 resultant particle type as a function of particle size and asymmetry. A discussion of thresholding
160 strategy is given, with emphasis on how varying strategies can influence characterization of
161 fluorescent properties and either under- or over-prediction of fluorescent biological particle
162 concentration.

163 **2. WIBS Instrumentation**

164 **2.1 Instrument Design and Operation**

165 The WIBS (Droplet Measurement Technologies; Longmont, Colorado) uses light scattering
166 and fluorescence spectroscopy to detect, size, and characterize the properties of interrogated
167 aerosols on a single particle basis (instrument model 4A utilized here). Air is drawn into the
168 instrument at a flow rate of 0.3 L/min and surrounded by a filtered sheath flow of 2.2 L/min. The
169 aerosol sample flow is then directed through an intersecting a 635 nm, continuous wave (cw)
170 diode laser, which produces elastic scattering measured in both the forward and side directions.
171 Particle sizing in the range of approximately 0.5 μm to 20 μm is detected by the magnitude of



172 the electrical pulse detected by a photomultiplier tube (PMT) located at 90 degrees from the laser
173 beam. Particles whose measured cw laser-scattering intensity (particle size) exceed user-
174 determined trigger thresholds will trigger two xenon flash lamps (Xe1 and Xe2) to fire in
175 sequence, approximately 10 microseconds apart. The two pulses are optically filtered to emit at
176 280 nm and 370 nm, respectively. Fluorescence emitted by a given particle after each excitation
177 pulse is detected simultaneously using two PMT detectors. The first PMT is optically filtered to
178 detect the total intensity of fluorescence in the range 310-400 nm and the second PMT in the
179 range 420-650 nm. So for every particle that triggers xenon lamp flashes, Xe1 produces a signal
180 in the FL1 (310-400 nm) and FL2 (420-650 nm) channels, whereas the Xe2 produces only a
181 signal in the FL3 (420-650 nm) channel because elastic scatter from the Xe2 flash saturates the
182 first PMT. The WIBS-4A has two user defined trigger thresholds, T1 and T2 that define which
183 data will be recorded. Particles producing a scattering pulse from the cw laser that is below the
184 T1 threshold will not be recorded. This enables the user to reduce data collection during
185 experiments with high concentrations of small particles. Particles whose scattering pulse exceeds
186 the T2 threshold will trigger xenon flash lamp pulses for interrogation of fluorescence. Note that
187 the triggering thresholds mentioned here are fundamentally different from the analysis thresholds
188 that will be discussed in detail later.

189 Forward-scattered light is detected using a quadrant PMT. The detected light intensity in
190 each quadrant are combined using Equation 1 into an asymmetry factor (AF), where k is an
191 instrument defined constant, E is the mean intensity measured over the entire PMT, and E_i is the
192 intensity measured at the i^{th} quadrant (Gabey et al., 2010).

$$193 \quad AF = \frac{k(\sum_{i=1}^n (E - E_i)^2)^{1/2}}{E} \quad (1)$$

194 This parameter relates to a rough estimate of the sphericity of an individual particle by
195 measuring the difference of light intensity scattered into each of the four quadrants. A perfectly
196 spherical particle would theoretically exhibit an AF value of 0, whereas larger AF values greater
197 than 0 and less than 100, indicate rod-like particles (Kaye et al., 1991; Gabey et al., 2010; Kaye et
198 al., 2005). It is important to note that this parameter is not rigorously a shape factor like used in
199 other aerosol calculations (DeCarlo et al., 2004; Zelenyuk et al., 2006) and only very roughly
200 relates a measure of particle sphericity.

201 **2.2 WIBS Calibration**

202 Particle sizing within the instrument was calibrated periodically by aerosolizing several sizes
203 of non-fluorescent polystyrene latex spheres (PSLs; Polysciences, Inc., Pennsylvania), including
204 0.51 μm (part number 07307), 0.99 μm . (07310), 1.93 μm (19814), 3.0 μm (17134), and 4.52 μm
205 (17135). A histogram of signal intensity was plotted separately for each PSL, and the peak of a
206 Gaussian fit to those data was then plotted versus the physical diameter of the PSL. A second
207 degree polynomial fit was used to generate an equation in order to calibrate side scatter values
208 into size.

209 Fluorescence intensity in each WIBS channel was calibrated using 2.0 μm Green (G0200),
210 2.1 μm Blue (B0200), and 2.0 μm Red (R0200) fluorescent PSLs (Thermo-Scientific,
211 Sunnyvale, California). For each particle type, a histogram of the fluorescence intensity signal in



212 each channel was fitted with a Gaussian function, and the median intensity was recorded.
213 Periodic checks were performed using the same stock bottles of the PSLs in order to verify that
214 mean fluorescence intensity of each had not shifted more than one standard deviation between
215 particle sample types (Table 1). The particle fluorescence standards used present limitations due
216 to variations in fluorescence intensity between stocks of particles and due to fluorophore
217 degradation over time. To improve reliability between instruments, stable fluorescence standards
218 and calibration procedures (e.g. Robinson et al., 2017) will be important.

219 Voltage gain settings for the three PMTs that produce sizing, fluorescence, and AF values,
220 respectively, significantly impact measured intensity values and are recorded here for rough
221 comparison of calibrations and analyses to other instruments. The voltage settings used for all
222 data presented here were set according to manufacturer specifications and are as follows: PMT₁
223 (AF) 400 V, PMT₂ (particle sizing and FL1 emission) 450 mV, and PMT₃ (FL2, FL3 emission)
224 732 mV.

225 2.3 WBS Data Analysis

226 An individual particle is considered to be fluorescent in any one of the three fluorescence
227 channels (FL1, FL2, or FL3) when its fluorescence emission intensity exceeds a given baseline
228 threshold. The baseline fluorescence can be determined by a number of strategies, but commonly
229 has been determined by measuring the observed fluorescence in each channel when the xenon
230 lamps are fired into the optical chamber when devoid of particles. This is referred to as the
231 “forced trigger” (FT) process, because the xenon lamp firing is not triggered by the presence of a
232 particle. The instrument background is also dependent on the intensity and orientation of Xe
233 lamps, voltage gains of PMTs, quality of PMTs based on production batch, orientation of optical
234 components i.e. mirrors in the optical chamber, etc. As a result of these factors, the background
235 or baseline of a given instrument is unique and cannot be used as a universal threshold. All
236 threshold values used in this study can be listed in supplementary Table S1. Fluorescence
237 intensity in each channel is recorded at an approximate FT rate of one value per second for a
238 user-defined time period, typically 30-120 seconds. The baseline threshold in each channel has
239 typically been determined as the average plus 3x the standard deviation (σ) of forced trigger
240 fluorescence intensity measurement (Gabey et al., 2010), however alternative applications of the
241 fluorescence threshold will be discussed. Particles exhibiting fluorescence intensity lower than
242 the threshold value in each of the three channels are considered to be non-fluorescent. The
243 emission of fluorescence from any one channel is essentially independent of the emission in the
244 other two channels. The pattern of fluorescence measured allows particles to be categorized into
245 7 fluorescent particle types (A, B, C, AB, AC, BC, or ABC) as depicted in Figure 1, or as
246 completely non-fluorescent (Perring et al., 2015).

247 Other threshold strategies have also been proposed and will be discussed. For example,
248 Wright et al. (2014) used set fluorescence intensity value boundaries rather than using the
249 standard Gabey et al. (2010) definition that applies a threshold as a function of observed
250 background fluorescence. The Wright et al. (2014) study proposed five separate categories of
251 fluorescent particles (FP1 through FP5). Each definition was determined by selecting criteria for
252 excitation-emission boundaries and observing the empirical distribution of particles in a 3-
253 dimensional space (FL1 vs. FL2 vs. FL3). For the study reported here, only the FP3 definition
254 was used for comparison, because Wright et al. (2014) postulated the category as being enriched



255 with fungal spores during their ambient study and because they observed that these particles
256 scaled more tightly with observed ice nucleating particles. The authors classified a particle in the
257 FP3 category if the fluorescence intensity in FL1 > 1900 arbitrary units (a.u) and between 0-500
258 a.u for each FL2 and FL3.

259 **3. Materials and methods**

260 **3.1 Aerosol Materials**

261 *3.1.1 Table of materials*

262 All materials utilized, including the vendors and sources from where they were acquired,
263 have been listed in supplemental Table S1, organized into broad particle type groups: biological
264 material (fungal spores, pollen, bacteria, and biofluorophores) and non-biological material (dust,
265 humic-like substances or HULIS, polycyclic aromatic hydrocarbons or PAHs, combustion soot
266 and smoke, and miscellaneous non-biological materials). Combustion soot and smoke are
267 grouped into one set of particles analyzed and are hereafter referred to as “soot” samples.

268 *3.1.2 Brown carbon synthesis*

269 Three different brown carbon solutions were synthesized using procedures described by
270 Powelson et al. (2014): (Rxn 1) methylglyoxal + glycine, (Rxn 2) glycolaldehyde +
271 methylamine, and (Rxn 3) glyoxal + ammonium sulfate. Reactions conditions were reported
272 previously, so only specific concentration and volumes used here are described. All solutions
273 described are aqueous and were dissolved into 18.2 MΩ water (Millipore Sigma; Denver, CO).
274 For reaction 1, 25.0 mL of 0.5 M methylglyoxal solution was mixed with 25 mL of 0.5 M
275 glycine solution. For reaction 2, 5.0 mL of 0.5 M glyoxal trimer dihydrate solution was mixed
276 with 5.0 mL of 0.5 M ammonium sulfate solution. For reaction 3, 10.0 mL of 0.5 M
277 glycolaldehyde solution was mixed with 10.0 mL of 0.5 M methylamine solution. The pH of the
278 solutions was adjusted to approximately pH 4 by adding 1 M oxalic acid in order for the reaction
279 to follow the appropriate chemical mechanism (Powelson et al., 2014). The solutions were
280 covered with aluminum foil and stirred at room temperature for 8 days, 4 days, and 4 days, for
281 reactions 1, 2, and 3, respectively. Solutions were aerosolized via the liquid aerosolization
282 method described in Section 3.2.4.

283 **3.2 Aerosolization Methods**

284 *3.2.1 Fungal spore growth and aerosolization*

285 Fungal cultures were inoculated onto sterile, disposable polystyrene plates (Carolina,
286 Charlotte, NC) filled with agar growth media consisting of malt extract medium mixed with
287 0.04 M of streptomycin sulfate salt (S6501, Sigma-Aldrich) to suppress bacterial colony growth.
288 Inoculated plates were allowed to mature and were kept in a sealed Plexiglas box for 3-5 weeks
289 until aerosolized. Air conditions in the box were monitored periodically and were consistently
290 25-27 °C and 70% relative humidity.

291 Fungal cultures were aerosolized inside an environmental chamber constructed from a re-
292 purposed home fish tank (Aqueon Glass Aquarium, 5237965). The chamber has glass panels



293 with dimensions 20.5 L x 10.25 H x 12.5 W in (supplemental Fig. S1). Soft rubber beading seals
294 the top panel to the walls, allowing isolation of air and particles within the chamber. Two tubes
295 are connected to the lid. The first delivers pressurized and particle-free air through a bulkhead
296 connection, oriented by plastic tubing (Loc-Line Coolant Hose, 0.64 inch outer diameter) and a
297 flat nozzle. The second tube connects 0.75 inch internal diameter conductive tubing (Simolex
298 Rubber Corp., Plymouth, MI) for aspiration of fungal aerosol, passing it through a bulkhead
299 fitting and into tubing directed toward the WIBS. Aspiration tubing is oriented such that a gentle
300 90-degree bend brings aerosol up vertically through the top panel.

301 For each experiment, an agar plate with a mature fungal colony was sealed inside the
302 chamber. The air delivery nozzle was positioned so that a blade of air was allowed to approach
303 the top of the spore colony at a shallow angle in order to eject spores into an approximately
304 horizontal trajectory. The sample collection tube was positioned immediately past the fungal
305 plate to aspirate aerosolized fungal particles. Filtered room air was delivered by a pump through
306 the aerosolizing flow at approximately 9 – 15 L/min, varied within each experiment to optimize
307 measured spore concentration. Sample flow was 0.3 L/min into the WIBS and excess input flow
308 was balanced by outlet through a particle filter connected through a bulkhead on the top plate.

309 Two additional rubber septa in the top plate allow the user to manipulate two narrow metal
310 rods to move the agar plate once spores were depleted from a given region of the colony. After
311 each spore experiment, the chamber and tubing was evacuated by pumping for 15 minutes, and
312 all interior surfaces were cleaned with isopropanol to avoid contamination between samples.

313 3.2.2 Bacterial growth and aerosolization

314 All bacteria were cultured in nutrient broth (Becton, Dickinson and Company, Sparks, MD)
315 for 18 hours in a shaking incubator at 30°C for *Bacillus atrophaeus* (ATCC 49337, American
316 Type Culture Collection, MD), 37°C for *Escherichia coli* (ATCC 15597), and 26°C
317 *Pseudomonas fluorescens* (ATCC 13525). Bacterial cells were harvested by centrifugation at
318 7000 rpm (6140 g) for 5 min at 4°C (BR4, Jouan Inc., Winchester, VA) and washed 4 times with
319 autoclave-sterilized deionized water (Millipore Corp., Billerica, MA) to remove growth media.
320 The final liquid suspension was diluted with sterile deionized water, transferred to a
321 polycarbonate jar and aerosolized using a three jet Collison nebulizer (BGI Inc., Waltham, MA)
322 operated at 5 L/min (pressure of 12 psi). The polycarbonate jar was used to minimize damage to
323 bacteria during aerosolization (Zhen et al., 2014). The tested airborne cell concentration was
324 about $\sim 10^5$ cells/Liter as determined by an optical particle counter (model 1.108, Grimm
325 Technologies Inc., Douglasville, GA). Bacterial aerosolization took place in an experimental
326 system containing a flow control system, a particle generation system, and an air-particle mixing
327 system introducing filtered air at 61 L/min as described by Han et al. (2015).

328 3.2.3 Powder aerosolization

329 Dry powders were aerosolized by mechanically agitating material by one of several methods
330 mentioned below and passing filtered air across a vial containing the powder. For each method,
331 approximately 2.5-5.0 g of sample was placed in a 10 mL glass vial. For most samples (method
332 P1), a stir bar was added, and the vial was placed on a magnetic stir plate. Two tubes were
333 connected through the lid of the vial. The first tube connected a filter, allowing particle-free air



334 to enter the vessel. The second tube connected the vial through approximately 33 cm of
335 conductive tubing (0.25 in inner diam.) to the WIBS for sample collection.

336 The setup was modified (method P2) for a small subset of samples whose solid powder was
337 sufficiently fine to produce high number concentrations of submicron aerosol particles that could
338 risk coating the internal flow path and damaging optical components of the instrument. In this
339 case, the same small vial with powder and stir bar was placed in a larger reservoir (~0.5 L), but
340 without vial lid. The lid of the larger reservoir was connected to filtered air input and an output
341 connection to the instrument. The additional container volume allowed for greater dilution of
342 aerosol before sampling into the instrument.

343 Some powder samples produced consistent aerosol number concentration even without
344 stirring. For these samples, 2.5 – 5.0 g of material was placed in a small glass vial and set under a
345 laboratory fume hood (method P3). Conductive tubing was held in place at the opening of the
346 vial using a clamp, and the opposite end was connected to the instrument with a flow rate of 0.3
347 L/min. The vial was tapped by hand or with a hand tool, physically agitating the material and
348 aerosolizing the powder.

349 *3.2.4 Liquid aerosolization*

350 Disposable, plastic medical nebulizers (Allied Healthcare, St. Louis, MO) were used to
351 aerosolize liquid solutions and suspensions. Each nebulizer contains a reservoir where the
352 solution is held. Pressurized air is delivered through a capillary opening on the side, reducing
353 static pressure and, as a result, drawing fluid into the tube. The fluid is broken up by the air jet
354 into a dispersion of droplets, where most of the droplets are blown onto the internal wall of the
355 reservoir, and droplets remaining aloft are entrained into the sample stream. Output from the
356 medical nebulizer was connected to a dilution chamber (aluminum enclosure, 0.5 L), allowing
357 the droplets to evaporate in the system before particles enter the instrument for detection.

358 *3.2.5 Smoke generation*

359 Wood and cigarette smoke samples were aerosolized through combustion. Each sample was
360 ignited separately using a personal butane lighter while held underneath a laboratory fume hood.
361 Once the flame from the combusting sample was naturally extinguished, the smoldering sample
362 was waved at a height ~5 cm above the WIBS inlet for 3– 5 minutes during sampling.

363 **3.3 Pollen microscopy**

364 Pollen samples were aerosolized using the dry powder vial (P1, P2) and tapping (P3)
365 methods detailed above. Samples were also collected by impaction onto a glass microscope slide
366 for visual analysis using a home-built, single-stage impactor with D_{50} cut ~0.5 μm at flow-rate
367 1.2 L min^{-1} . Pollen were analyzed using an optical microscope (VWR model 89404-886) with a
368 40x objective lens. Images were collected with an AmScope complementary metal-oxide
369 semiconductor camera (model MU800, 8 megapixels).

370 **4. Results**

371 **4.1 Broad separation of particle types**



372 The WIBS is routinely used as an optical particle counter applied to the detection and
373 characterization of fluorescent biological aerosol particles (FBAP). Each interrogated particle
374 provides five discreet pieces of information: fluorescence emission intensity in each of the 3
375 detection channels (FL1, FL2, and FL3), particle size, and particle asymmetry. Thus, a thorough
376 summary of data from aerosolized particles would require the ability to show statistical
377 distributions in five dimensions. As a simple, first-order representation of the most basic
378 summary of the 69 particle types analyzed, Figure 2 and Table 1 show median values for each of
379 the five data parameters plotted in three plot styles (columns of panels in Fig. 2).

380 For the sake of WIBS analysis, each pollen type was broken into two size categories, because
381 it was observed that most pollen species exhibited two distinct size modes. The largest size mode
382 peaked above 10 μm in all cases and often saturated the sizing detector (see also fraction of
383 particles that saturated particle detector for each fluorescence channel in Table 2). This was
384 interpreted to be intact pollen. A broad mode also usually appeared at smaller particle diameters
385 for some pollen species, suggesting that pollen grains had ruptured during dry storage or through
386 the mechanical agitation process. This hypothesis was supported by optical microscopy through
387 which a mixture of intact pollen grains and ruptured fragments were observed (Fig. S2). For the
388 purposes of this investigation, the two modes were separated at the minimum point between
389 modes in order to observe optical properties of the intact pollen and pollen fragments separately.
390 The list number for each pollen (Tables 2, S1) is consistent for the intact and fragmented species,
391 though not all pollen exhibited obvious pollen fragments.

392 The WIBS was developed primarily to discriminate biological from non-biological particles,
393 and the three fluorescence channels broadly facilitate this separation. Biological particles, i.e.
394 pollen, fungal spores, and bacteria (top row of Fig. 2), each show strong median fluorescence
395 signal in at least one of the three channels. In general, all fungal spores sampled (blue dots) show
396 fluorescence in the FL1 channel with lower median emission in FL2 and FL3 channels. Both the
397 fragmented (pink dots) and intact (orange dots) size fractions of pollen particles showed high
398 median fluorescence emission intensity in all channels, varying by species and strongly as a
399 function of particle size. The three bacterial species sampled (green dots) showed intermediate
400 median fluorescence emission in the FL1 channel and very low median intensity in either of the
401 other two channels. To support the understanding of whole biological particles, pure molecular
402 components common to biological material were aerosolized separately and are shown as the
403 second row of Figure 2. Each of the biofluorophores chosen shows relatively high median
404 fluorescence intensity, again varying as a function of size. Key biofluorophores such as NAD,
405 riboflavin, tryptophan, and tyrosine are individually labeled in Figure 2d. Supermicron particles
406 of these pure materials would not be expected in a real-world environment, but are present as
407 dilute components of complex biological material and are useful here for comparison. In general,
408 the spectral properties summarized here match well with fluorescence excitation emission
409 matrices (EEMs) presented by Pöhlker et al. (2012;2013)

410 In contrast to the particles of biological origin, a variety of non-biological particles were
411 aerosolized in order to elucidate important trends and possible interferences. The majority of
412 non-biological particles shown in the bottom row of Figure 2 show little to no median
413 fluorescence in each channel and are therefore difficult to differentiate from one another in the
414 figure. For example, Figure 2g (lower left) shows the median fluorescence intensity of 6 different
415 groups of particle types (33 total dots), but almost all overlap at the same point at the graph



416 origin. The exceptions to this trend include the PAHs (blue dots), miscellaneous particles (green)
417 and several types of combustion soot (black dots). The fluorescent properties of PAHs are well-
418 known in both basic chemical literature and as observed in the atmosphere (Niessner and Krupp,
419 1991; Finlayson-Pitts and Pitts, November 1999; Panne et al., 2000; Slowik et al., 2007). PAHs
420 can be produced by a number of anthropogenic sources and are emitted in the exhaust from
421 vehicles and other combustion sources as well as from biomass burning (Aizawa and Kosaka,
422 2010, 2008; Abdel-Shafy and Mansour, 2016; Lv et al., 2016). PAHs alone exhibit high
423 fluorescence quantum yields (Pöhlker et al., 2012; Mercier et al., 2013), but as pure materials are
424 not usually present in high concentrations at sizes large enough ($>0.8 \mu\text{m}$) to be detected by the
425 WIBS. Highly fluorescent PAH molecules are also common constituents of other complex
426 particles, including soot particle agglomerates. It has been observed that the fluorescent emission
427 of PAH constituents on soot particles can be weak due to quenching from the bulk material
428 (Panne et al., 2000). Several examples of soot particles shown in Figure 2g are fluorescent in
429 FL1 and indeed should be considered as interfering particle types, as will be discussed. Three
430 miscellaneous particles (laboratory wipes and two colors of cotton t-shirts) were also
431 interrogated by rubbing samples over the WIBS inlet, because of their relevance to indoor
432 aerosol investigation (e.g. Bhangar et al., 2014; Handorean et al., 2015; e.g. Bhangar et al., 2016).
433 These particles (dark blue dots, Fig. 2 bottom row) show varying median intensity in FL1,
434 suggesting that sources such as tissues, cleaning wipes, and cotton clothing could be sources of
435 fluorescent particles within certain built environments.

436 Another interesting point from the observations of median fluorescence intensity is that the
437 three viable bacteria aerosolized in this study each shows moderately fluorescent characteristics
438 in FL1 and low fluorescent characteristics in FL2 and FL3 (Fig. 2a-c). A study by Hernandez et
439 al. (2016) also focused on analysis strategies using the WIBS and shows similar results regarding
440 bacteria. Of the 14 bacteria samples observed in the Hernandez et al. study, 13 were categorized
441 as predominantly A-type particles, thus meaning they exhibited fluorescent properties in FL1 and
442 only a very small fraction of particles showed fluorescence above the applied threshold ($FT +$
443 3σ) in either FL2 or FL3. The FL3 channel in the WIBS-4A has an excitation of 370 nm and
444 emission band of 420-650 nm, similar to that of the UV-APS with an excitation of 355 nm and
445 emission band of 420-575 nm. Previous studies have suggested that viable microorganisms (i.e.
446 bacteria) show fluorescence characteristics in the UV-APS due to the excitation source of 355
447 nm that was originally designed to excite NAD(P)H and riboflavin molecules present in actively
448 metabolizing organisms (Agranovski et al., 2004; Hairston et al., 1997; Ho et al., 1999; Pöhlker et
449 al., 2012). Previous studies with the UV-APS and other UV-LIF instruments using
450 approximately similar excitation wavelengths have shown a strong sensitivity to the detection of
451 “viable” bacteria (Hill et al., 1999b; Pan et al., 1999; Hairston et al., 1997; Brosseau et al., 2000).
452 Because the bacteria here were aerosolized and detected immediately after washing from growth
453 media, we expect that a high fraction of the bacterial signal was a result of living vegetative
454 bacterial cells. The results presented here and from other studies using WIBS instruments, in
455 contrast to reports using other UV-LIF instruments, suggest that the WIBS-4A is highly sensitive
456 to the detection of bacteria using 280 nm excitation (only FL1 emission), but less so using the
457 370 nm excitation (FL3 emission) (e.g. Perring et al., 2015; Hernandez et al., 2016). A study by
458 Agranovski et al. (2003) also demonstrated that the UV-APS was limited in its ability to detect
459 endospores (reproductive bacterial cells from spore-forming species with little or no metabolic
460 activity and thus low NAD(P)H concentration). The lack of FL3 emission observed from
461 bacteria in the WIBS may also suggest a weaker excitation intensity in Xe2 with respect to Xe1,



462 manifesting in lower overall FL3 emission intensity (Könemann et al., In Prep.). Gain voltages
463 applied differently to PMT2 and PMT3 could also impact differences in relative intensity
464 observed. Lastly, it has been proposed that the rapid sequence of Xe1 and Xe2 excitation could
465 lead to quenching of fluorescence from the first excitation flash, leading to overall reduced
466 fluorescence in the FL3 channel (Sivaprakasam et al., 2011). These factors may similarly affect
467 all WIBS instruments and should be kept in mind when comparing results here with other UV-
468 LIF instrument types.

469 **4.2 Fluorescence type varies with particle size**

470 The purpose of Figure 2 is to distill complex distributions of the five data parameters into a
471 single value for each in order to show broad trends that differentiate biological and non-
472 biological particles. By representing the complex data in such a simple way, however, many
473 relationships are averaged away and lost. For example, the histogram of FL1 intensity for fungal
474 spore *Aspergillus niger* (Fig. S3) shows a broad distribution with long tail at high fluorescence
475 intensity, including ca. ~ 6 % of particles that saturate the FL1 detector (Table S2). If a given
476 distribution were perfectly Gaussian and symmetric, the mean and standard deviation values
477 would be sufficient to fully describe the distribution. However, given that asymmetric
478 distributions often include detector-saturating particles, no single statistical fit characterizes data
479 for all particle types well. Median values were chosen for Figure 2 knowing that the resultant
480 values can reduce the physical meaning in some cases. For example, the same *Aspergillus niger*
481 particles show a broad FL1 peak at ~150 a.u. and another peak at 2047 a.u. (detector saturated),
482 whereas the median FL1 intensity is 543 a.u., at which point there is no specific peak. In this
483 way, the median value only broadly represents the data by weighting both the broad distribution
484 and saturating peak. To complement the median values, however, Table 1 also shows the fraction
485 of particles that were observed to saturate the fluorescence detector in each channel.

486 The representation of median values for each of the five parameters (Fig. 2) shows broad
487 separation between particle classes, but discriminating more finely between particle types with
488 similar properties by this analysis method can be practically challenging. Rather than
489 investigating the intensity of fluorescence emission in each channel, however, a common method
490 of analyzing field data is to apply binary categorization for each particle in each fluorescence
491 channel. For example, by this process, a particle is either fluorescent in a given FL channel
492 (above emission intensity threshold) or non-fluorescent (below threshold). In this way, many of
493 the challenges of separation introduced above are significantly reduced, though others are
494 introduced. Perring et al. (2015) introduced a WIBS classification strategy by organizing
495 particles sampled by the WIBS as either non-fluorescent or into one of seven fluorescence types
496 (e.g. Fig. 1).

497 Complementing the perspective from Figure 2, stacked particle type plots (Fig. 3) show
498 qualitative differences in fluorescence emission by representing different fluorescence types as
499 different colors. The most important observation here is that almost all individual biological
500 particles aerosolized (top two rows of Fig. 3) are fluorescent, meaning that they exhibit
501 fluorescence emission intensity above the standard threshold (FT baseline + 3σ) in at least one
502 fluorescence channel and are depicted with a non-gray color. Figure S4 shows the stacked
503 particle type plots for all 69 materials analyzed in this study as a comprehensive library. In
504 contrast to the biological particles, most particles from non-biological origin were observed not



505 to show fluorescence emission above the threshold in any of the fluorescence channels and are
506 thus colored gray. For example, 11 of the 15 samples of dust aerosolized show <15% of particles
507 to be fluorescent at particle sizes <4 μm . Similarly, 4 of 5 samples of HULIS aerosolized show
508 <7 % of particles to be fluorescent at particle sizes <4 μm . The size cut-point here was chosen
509 arbitrarily to summarize the distributions. Two examples shown in Figure 3 (Dust 10 and HULIS
510 3) are representative of average dust and HULIS types analyzed, respectively, and are relatively
511 non-fluorescent. Of the four dust types that exhibit a higher fraction of fluorescence, two (Dust 3
512 and Dust 4) are relatively similar and show ~75% fluorescent particles <4 μm , with particle type
513 divided nearly equally across the A, B, and AB particle types (Fig. S4I). The two others (Dust 2
514 and Dust 6) show very few similarities between one another, where Dust 2 shows size-dependent
515 fluorescence and Dust 6 shows particle type A and B at all particle sizes (Fig. S4I). As seen by
516 the median fluorescence intensity representation (Fig. 2, Table 1), however, the relative intensity
517 in each channel for all dusts is either below or only marginally above the fluorescence threshold.
518 Thus, the threshold value becomes critically important and can dramatically impact the
519 classification process, as will be discussed in a following section. Similarly, HULIS 5 (Fig. S4K)
520 is the one HULIS type that shows an anomalously high fraction of fluorescence, and is
521 represented by B, C, BC particle types, but at intensity only marginally above the threshold value
522 and at 0% detector saturation in each channel.

523 Several types of non-biological particles, specifically brown carbon and combustion soot and
524 smoke, exhibited higher relative fractions of fluorescent particles compared to other non-
525 biological particles. Two of the three types of brown carbon sampled show >50% of particles to
526 be fluorescent at sizes >4 μm (Figs. 3i, l), though their median fluorescence is relatively low and
527 neither shows saturation in any of the three fluorescent channels. Out of six soot samples
528 analyzed, four showed >69% of particles to be fluorescent at sizes >4 μm , most of which are
529 dominated by B particle types. Two samples of combustion soot are notably more highly
530 fluorescent, both in fraction and intensity. Soot 3 (fullerene soot) and Soot 4 (diesel soot) show
531 FL1 intensity of 318 a.u. and 751 a.u., respectively, and are almost completely represented as A
532 particle type. The fullerene soot is not likely a good representative of most atmospherically
533 relevant soot types, however diesel soot is ubiquitous in anthropogenically-influenced areas
534 around the world. The fact that it exhibits high median fluorescence intensity implies that
535 increasing the baseline threshold slightly will not appreciably reduce the fraction of particles
536 categorized as fluorescent, and these particles will thus be counted as fluorescent in many
537 instances. The one type of wood smoke analyzed (Soot 6) shows ca. 70% fluorescent at >4 μm ,
538 mostly in the B category, with moderate to low FL2 signal, and also presents similarly as
539 cigarette smoke. Additionally, the two smoke samples in this study (Soot 5, cigarette smoke and
540 Soot 6, wood smoke) share similar fluorescent particle type features with two of the brown
541 carbon samples BrC 1 and BrC2. The smoke samples are categorized predominantly as B-type
542 particles, whereas samples more purely comprised of soot exhibit predominantly A-type
543 fluorescence. This distinction between smoke and soot may arise partially because the smoke
544 particles are complex mixtures of amorphous soot with condensed organic liquids, indicating that
545 compounds similar to the brown carbon analyzed here could heavily influence the smoke particle
546 signal.

547 Biological particle types were chosen for Figure 3 to show the most important trends among
548 all particle types analyzed. Two pollen are shown here to highlight two common types of
549 fluorescence properties observed. Pollen 9 (Fig. 3a) shows particle type transitioning between A,



550 AB, and ABC as particle size gets larger. Pollen 9 (*Phleum pretense*) has a physical diameter of
551 $\sim 35 \mu\text{m}$, so the mode seen in Figure 3a may be a result of fragmented pollen and due to the upper
552 particle size limit of WIBS detection, intact pollen cannot be detected (Pöhlker et al., 2013).
553 Pollen 8 (Fig. 3d) shows a mode peaking at $\sim 10 \mu\text{m}$ in diameter and comprised of a mixture of
554 B, AB, BC, and ABC particles as well as a larger particle mode comprised of ABC particles. The
555 large particle mode appears almost monodisperse, but this is due to the WIBS ability to sample
556 only the tail of the distribution due to the upper size limit of particle collection ($\sim 20 \mu\text{m}$ as
557 operated). It is important to note that excitation pulses from the Xe flash lamps are not likely to
558 penetrate the entirety of large pollen particles, and so emission information is likely limited to
559 outer layers of each pollen grain. Excitation pulses can penetrate a relatively larger fraction of
560 the smaller pollen fragments, however, meaning that the differences in observed fluorescence
561 may arise from differences the layers of material interrogated. Fungi 1 (Fig. 3b) was chosen
562 because it depicts the most commonly observed fluorescence pattern among the fungal spore
563 types analyzed ($\sim 3 \mu\text{m}$ mode mixed with A and AB particles). Fungi 4 (Fig. 3e) represents a
564 second common pattern (particle size peaking at larger diameter, minimal A-type, and dominated
565 by AB, ABC particle types). All three bacteria types analyzed were dominated by A-type
566 fluorescence. One gram-positive (Bacteria 1) and one gram-negative bacteria (Bacteria 3) types
567 are shown in Figure 3c, f, respectively.

568 4.3 Fluorescence intensity varies strongly with particle size

569 An extension of observation from the many particle classes analyzed is that particle type (A,
570 AB, ABC, etc.) varies strongly as a function of particle size. This is not surprising, given that it
571 has been frequently observed and reported that particle size significantly impacts fluorescence
572 emission intensity (e.g. Hill et al., 2001; Sivaprakasam et al., 2011). The higher the fluorescent
573 quantum yield of a given fluorophore, the more likely it is to fluoresce. For example, pure
574 biofluorophores (middle row of Fig. 2) and PAHs (bottom row of Fig. 2) have high quantum
575 yields and thus exhibit relatively intense fluorescence emission, even for particles $< 1 \mu\text{m}$. In
576 contrast, more complex particles comprised of a wide mixture of molecular components are
577 typically less fluorescent per volume of material. At small sizes the relative fraction of these
578 particles that fluoresce is small, but as particles increase in size they are more likely to contain
579 enough fluorophores to emit a sufficient number of photons to record an integrated light intensity
580 signal above a given fluorescence threshold. Thus, the observed fluorescence intensity scales
581 approximately between the 2nd and 3rd power of the particle diameter (Sivaprakasam et al.,
582 2011; Taketani et al., 2013; Hill et al., 2015).

583 The general trend of fluorescence dependence on size is less pronounced for FL1 than for
584 FL2 and FL3. This can be seen by the fact that the scatter of points along the FL1 axis in Figure
585 2b is not clearly size-dependent and is strongly influenced by particle type (i.e. composition
586 dependent). In Figure 2c, however, the median points cluster near the vertical (size) axis and
587 both FL2 and FL3 values increase as particle size increases. It is important to note, however, that
588 the method chosen for particle generation in the laboratory strongly impacts the size distribution
589 of aerosolized particles. For example, higher concentrations of an aqueous suspension of particle
590 material generally produce larger particles, and the mechanical force used to agitate powders or
591 aerosolize bacteria can have strong influences on particle viability and physical agglomeration or
592 fragmentation of the aerosol (Mainelis et al., 2005). So, while the absolute size of particles
593 shown here is not a key message, the relative fluorescence at a given size can be informative.



594 As discussed, each individual particle shows increased probability of exhibiting fluorescence
595 emission above a given fluorescence threshold as size increases. Using Pollen 9 (*Phleum*
596 *pratense*, Fig. 3a) as an example, most particles $<3\ \mu\text{m}$ show fluorescence in only the FL1
597 channel and are thus classified as A-type particles. For the same pollen, however, particles ca. 2-
598 $6\ \mu\text{m}$ in diameter are more likely to be recorded as AB-type particles, indicating that they have
599 retained sufficient FL1 intensity, but have exceeded the FL2 threshold to add B-type
600 fluorescence character. Particles larger still ($>4\ \mu\text{m}$) are increasingly likely to exhibit ABC
601 character, meaning that the emission intensity in the FL3 channel has increased to cross the
602 fluorescence threshold. Thus, for a given particle type and a constant threshold as a function of
603 particle size, the relative breakdown of fluorescence type changes significantly as particle size
604 increases. The same general trend can be seen in many other particle types, for example Pollen 8
605 (*Alnus glutinosa*, Fig. 3d), Fungi 1 (*Aspergillus brasiliensis*, Fig. 3b), and to a lesser degree
606 HULIS 3 (Suwannee fulvic acid, Fig. 3j) and Brown Carbon 2 (Fig. 3i). The “pathway” of
607 change, for Pollen 9, starts as A-type at small particle size and adds B and eventually ABC
608 ($A \rightarrow AB \rightarrow ABC$), whereas Pollen 8 starts primarily with B-type at small particle size and
609 separately adds either B or C en route to ABC ($B \rightarrow AB$ or $BC \rightarrow ABC$). In this way, not only is
610 the breakdown of fluorescence type useful in discriminating particle distributions, but the
611 pathway of fluorescence change with particle size can also be instructive.

612 To further highlight the relationship between particle size and fluorescence, four kinds of
613 particles (Dust 2, HULIS 5, Fungi 4, and Pollen 9) were each binned into 4 different size ranges,
614 and the relative number fraction was plotted versus fluorescence intensity signal for each channel
615 (Fig. 4). In each case, the fluorescence intensity distribution shifts to the right (increases) as the
616 particle size bin increases. This trend is strongest in the FL2 and FL3 (middle and right columns
617 of Fig. 4) for most particle types, as discussed above.

618 The fact that particle fluorescence type can change so dramatically with increasing particle
619 size becomes critically important when the Perrin-style particle type classification is utilized for
620 laboratory or field investigation. For example Hernandez et al. (2016) aerosolized a variety of
621 species of pollen, fungal spores, and bacteria in the laboratory and presented the break-down of
622 particle types for each aerosolized species. This first comprehensive overview summarized how
623 different types of biological material (i.e. pollen and bacteria) might be separated based on their
624 fluorescence properties when presented with a population of relatively monodisperse particles.
625 This was an important first step, however, differentiation becomes more challenging when broad
626 size distributions of particles are mixed in an unknown environment. In such a case,
627 understanding how the particle type may change as a function of particle size may become an
628 important aspect of analysis.

629 **4.4 Fluorescence threshold defines particle type**

630 Particle type analysis is not only critically affected by size, but also by the threshold
631 definition chosen. Figure 5 represents the same matrix of particle types as in Figure 3, but shows
632 the fluorescence intensity distribution in each channel (at a given narrow range of sizes in order
633 to minimize the sizing effect on fluorescence). Figure 5 can help explain the breakdown of
634 particle type (and associated colors) shown in Figure 3. For example, in Figure 5a, the median
635 fluorescence intensity in FL1 for Pollen 9 (2046 a.u., detector saturated) in the size range 3.5-4.0
636 μm far exceeds the 3σ threshold (51 a.u.), and so essentially all particles exhibit FL1 character.



637 Approximately 90% of particles of Pollen 9 are above the 3σ FL2 threshold (25 a.u.), and
638 approximately 63% of particles are above the 3σ FL3 threshold (49 a.u). These three channels of
639 information together describe the distribution of particle type at the same range of sizes: 9% A,
640 26% AB, 63% ABC, and 2% other categories. Since essentially all particles are above the
641 threshold for FL1, particles are thus assigned as A type particles (if $< FL2$ and $FL3$ thresholds),
642 AB (if $> FL2$ threshold and $< FL3$ threshold), or ABC (if $> FL2$ and $FL3$ thresholds). Thus, the
643 distribution of particles at each fluorescence intensity and in relation to a given thresholding
644 strategy defines the fluorescence type breakdown and the pathway of fluorescence change with
645 particle size. It is important to note differences in this pathway for biofluorophores (Figs. S4G
646 and S4H). For example Biofluorophore 1 (riboflavin) follows the pathway $B \rightarrow C \rightarrow BC$ while
647 Biofluorophore 11 (tryptophan) follows the pathway $A \rightarrow BC \rightarrow ABC$.

648 By extension, the choice of threshold bears heavily on how a given particle breakdown
649 appears and thus how a given instrument may be used to discriminate between biological and
650 non-biological particles. A commonly made assumption is that particles exhibiting fluorescence
651 by the WBS (or UV-APS) can be used as a lower limit proxy to the concentration of biological
652 particles, though it is known that interfering particle types confound this simple assumption
653 (Huffman et al., 2010). Increasing the fluorescence threshold can reduce categorizing weakly
654 fluorescent particles as biological, but can also remove weakly fluorescing biological particles of
655 interest (Huffman et al., 2012). Figure 6 provides an analysis of 8 representative particle types (3
656 biological, 5 non-biological) in order to estimate the trade-offs of increasing fluorescence
657 threshold separately in each channel. Once again, the examples chosen here represent general
658 trends and outliers, as discussed previously for Figure 3. Four threshold strategies are presented:
659 three as the instrument fluorescence baseline plus increasing uncertainty on that signal ($FT + 3\sigma$,
660 $FT + 6\sigma$, and $FT + 9\sigma$), as well as the FP3 strategy suggested by Wright et al. (2014). Using Dust
661 4 as an example (Fig. 6d), by increasing the threshold from 3σ (red traces) to 6σ (orange traces),
662 the fraction of dust particles fluorescent in FL1 decreases from approximately 50% to 10%.
663 Increasing the fluorescence threshold even higher to 9σ , reduces the fraction of fluorescence to
664 approximately 1%, thus eliminating nearly all interfering particles of Dust 3. In contrast, for
665 biological particles such as Pollen 9 (Fig. 6b), increasing the threshold from 3σ to 9σ does very
666 little to impact the relative breakdown of fluorescence category or the fraction of particles
667 considered fluorescent in at least one channel. Changing threshold from 3σ to 9σ decreases the
668 FL1 fraction minimally (98.3% to 97.9%), and for FL2 and FL3 the fluorescence fraction
669 decreases from 90% to 50% and from 60% to 42%, respectively. Figure 6 also underscores how
670 increasing particle size affects fluorescence fraction, as several particle types (e.g. Pollen 9 and
671 HULIS 5) show sigmoidal curves that proceed toward the right (lower fraction at a given size) as
672 the threshold applied increases and thus removes more weakly fluorescent particles.

673 To better understand how the different thresholding strategies qualitatively change the
674 distribution of particle fluorescence type, Figure 7 shows stacked fluorescence type distributions
675 for each of the four thresholds analyzed. Looking first at Dust 3 (Fig. 7d), the standard threshold
676 definition of 3σ shows approximately 80% of particles to be fluorescent in at least one channel,
677 resulting in a distribution of predominantly A, B, and AB-type particles. As the threshold is
678 increased, however, the total percentage of fluorescent particles decreases dramatically to 1% at
679 9σ and the particle type of the few remaining particles shifts to A-type particles. A similar trend
680 of fluorescent fraction can also be seen for Soot 6 (wood smoke) and Brown Carbon 2, where
681 almost no particle (10% and 16%, respectively) remain fluorescent using the 9σ threshold. Soot 4



682 (diesel soot), in contrast, exhibits the same fraction and breakdown of fluorescent particles
683 whether using the 3σ or 9σ threshold. Using the FP3 threshold (which employs very high FL1
684 threshold), however, the fluorescent properties of the diesel soot change dramatically to non-
685 fluorescent. As a ‘worst case’ scenario, HULIS 5 shows ca. 60% of particles to be fluorescent
686 using the 3σ threshold. In this case, increasing the threshold from 6σ to 9σ only marginally
687 decreases the fraction of fluorescent particles to ca. 35% and 22%, respectively, and the break-
688 down remains relatively constant in B, C, and BC types. Changing the threshold definition to
689 FP3 in this case also does not significantly change the particle type break-down, since the high
690 FP3 threshold applies only to FL1.

691 As stated, the WIBS is mostly often applied toward the detection and characterization of
692 biological aerosol particles. For the biological particles analyzed (Fig. 7, top rows), increasing
693 the threshold from 3σ to 9σ shows only a marginal decrease in the total fluorescent fraction for
694 Pollen 9, Fungal Spore 1, and Bacteria 1, and only a slight shift in fluorescence type as a
695 function of size. Using the FP3 threshold, however, for each of the three biological species the
696 non-fluorescent fraction increases substantially. Wright et al. (2014) found that the FP3 threshold
697 definition showed a strong correlation with ice nucleating particles and the authors suggested
698 these particles with high FL1 intensity were likely to be fungal spores. This may have been the
699 case, but given the analysis here, the FP3 threshold is also likely to significantly underestimate
700 fungal spore number by missing weakly or marginally fluorescent spores.

701 Based on the threshold analysis results shown in Figure 7, marginally increasing the
702 threshold in each case may help eliminate non-biological, interfering particles without
703 significantly impacting the number of biological particles considered fluorescent. Each threshold
704 strategy brings trade-offs, and individual users must understand these factors to make appropriate
705 decisions for a given scenario. These data suggest that using a threshold definition of FT baseline
706 + 9σ is likely to reduce interferences from most non-biological particles without significantly
707 impacting most biological particles.

708 **4.5 Particle asymmetry varies with particle size**

709 As a part of the comprehensive WIBS study, particle asymmetry (AF) was analyzed as a
710 function of particle size for all particles. As described in Section 2.1, AF in the WIBS-4A is
711 determined by comparing the symmetry of the forward elastic scattering response of each
712 particle, measured at the quadrant PMT. Many factors are related to the accuracy of the
713 asymmetry parameter, including the spatial alignment of the collection optics, signal-to-noise
714 and dynamic range of the detector, agglomeration of particles with different refractive indices,
715 and the angle at which a non-symmetrical particle hits the laser (Kaye et al., 2007; Gabey et al.,
716 2010). Figure 8 shows a summary of the relationship between AF and particle size for all
717 material types analyzed in Table 1. Soot particles are known to frequently cluster into chains or
718 rings depending on the number of carbon atoms (Von Helden et al., 1993) and, as a result, can
719 have long aspect ratios that would be expected to manifest as large AF values. The bacteria
720 species chosen have rod-like shape features and thus would also exhibit large AF values. These
721 properties were observed by the WIBS, as two types of soot (diesel and fullerene) and all three
722 bacteria showed higher AF values than other particles at approximately the same particle
723 diameter. For an unknown reason, all three brown carbon samples also showed relatively high
724 AF values given that the individual particles of liquid organic aerosol would be expected to be



725 spherical with low AF. Similarly, the intact pollen showed anomalously low AF, because a
726 substantial fraction of each was shown to saturate the WIBS sizing detector, even if the median
727 particle size (shown) is lower than the saturating value. For this reason we postulate that the side-
728 scattering detector may not be able to reliably estimate either particle size or AF when particles
729 are near the sizing limits. Intact pollen, soot samples (diesel and fullerene soot), bacteria and
730 brown carbon samples were excluded from the linear regression fit, because they appeared
731 visually as outliers to the trend. All remaining particle groups of material types (7 in total) are
732 represented by blue in Figure 8. A linear regression R^2 value of 0.87 indicates a high degree of
733 correlation between particle AF and size across the remaining particles. The strong correlation
734 between these two factors across a wide range of particle types, mixed with the confounding
735 anomaly of brown carbon, raises a question about the degree to which the asymmetry factor
736 parameter from the WIBS-4A can be useful or, conversely, to what degree the uncertainty in AF
737 is dominated by instrumental factors, including those listed above.

738 5. Summary and Conclusions

739 UV-LIF instruments, including the WIBS, are common tools for the detection and
740 characterization of biological aerosol particles. The number of commercially available
741 instruments regularly deployed for ambient monitoring of environmental particle properties is
742 rising steeply, yet critical laboratory work has been needed to better understand how the
743 instruments categorize a variety of both biological and non-biological particles. In particular, the
744 differentiation between weakly fluorescent, interfering particles of non-biological origin and
745 weakly fluorescing biological particles is very challenging. Here we have aerosolized a
746 representative list of pollen, fungal spores, and bacteria along with key aerosol types from the
747 groups of fluorescing non-biological materials expected to be most problematic for UV-LIF
748 instrumentation.

749 By analyzing the five WIBS data parameter outputs for each interrogated particle, we have
750 summarized trends within each class of particles and demonstrated the ability of the instrument
751 to broadly differentiate populations of particles. The trend of particle fluorescence intensity and
752 changing particle fluorescence type as a function of particle size was shown in detail. This is
753 critically important for WIBS and other UV-LIF instrumentation users to keep in mind when
754 analyzing populations of unknown, ambient particles. In particular, we show that the pathway of
755 fluorescence particle type change (e.g. $A \rightarrow AB \rightarrow ABC$ or $B \rightarrow BC \rightarrow ABC$) with increasing
756 particle size can be one characteristic feature of unique populations of particles. When
757 comparing the fluorescence break-down of individual aerosol material types, care should be
758 taken to limit comparison within a narrow range of particle sizes in order to reduce complexity
759 due to differing composition or fluorescence intensity effects.

760 The fluorescence threshold applied toward binary categorization of fluorescence or non-
761 fluorescent in each channel is absolutely critical to the conceptual strategy that a given user
762 applies to ambient particle analysis. A standard WIBS threshold definition of instrument
763 background (FT baseline) + 3σ is commonly applied to discriminate between particles with or
764 without fluorescence. As has been shown previously, however, any single threshold confounds
765 simple discrimination of biological and non-biological particles by mixing poorly fluorescent
766 biological material into non-fluorescent categories, and highly fluorescent non-biological
767 material into fluorescent categories. Previously introduced thresholding strategies were also used



768 for comparison. The Wright et al. (2014) definition was shown to aid in removing non-biological
769 particles such as soot, but that it can also lead to the dramatic underestimation of the biological
770 fraction. The strategy utilized by Toprak and Schnaiter (2013) was to define fluorescent
771 biological particles as those with fluorescent characteristics in FL1 and FL3, ignoring any
772 particles with fluorescence in FL2. They proposed this because FL1 shows excitation and
773 emission characteristics well suited for the detection of tryptophan, and FL3 for the detection of
774 NAD(P)H and riboflavin. However, the study here, along with studies by Hernandez et al. (2016)
775 and Perring et al. (2015), have shown that FL2 fluorescence characteristics (B, AB, BC, and
776 ABC type) are common for many types of biological particles and so removing particles with
777 FL2 fluorescence is likely to remove many bioparticles from characterization.

778 Any one threshold has associated trade-offs and is likely to create some fraction of both false
779 positive and false negative signals. Here we have shown a systematic analysis of four different
780 fluorescence thresholding strategies, concluding that by raising the threshold to $FT + 9\sigma$, the
781 reduction in biological material counted as fluorescent is likely to be only minimally effected,
782 while the fraction of interfering material is likely to be reduced almost to zero for most particle
783 types. Several materials exhibiting outlier behavior (e.g. HULIS 5, diesel soot) could present as
784 false positive counts using almost any characterization scheme. It is important to note that
785 HULIS 5 was one of a large number of analyzed particle types and in the minority of HULIS
786 types, however, and it is unclear how likely these highly fluorescent materials are to occur in any
787 given ambient air mass. More studies may be required to sample dusts, HULIS types, soot and
788 smoke, brown organic carbon materials, and various coatings in different real-world settings to
789 better understand how specific aerosol types may contribute to UV-LIF interpretation at a given
790 study location. We also included a comprehensive supplemental document including size
791 distributions for all 69 aerosol materials, stacked by fluorescent particle type and comparing the
792 $FT + 3\sigma$ and $FT + 9\sigma$ threshold strategies. These figures are included as a qualitative reference
793 for other instrument users when comparing against laboratory-generated particles or for use in
794 ambient particle interpretation.

795 It should be noted, however, that the presented assessment is not intended to be exhaustive,
796 but has the potential to guide users of commercial UV-LIF instrumentation through a variety of
797 analysis strategies toward the goal of better detecting and characterizing biological particles. One
798 important note is that the information presented here is strongly instrument dependent due to
799 fluorescence PMT voltages and gains, specific fluorescence calibrations applied, and other
800 instrument parameters (Robinson et al., 2017). For example, the suggested particle type
801 classification introduced by Perring et al. (2015), will vary somewhat between instruments,
802 though more work will be necessary to determine the magnitude of these changes. Thus, we do
803 not introduce these data primarily as a library to which all other WBS instrument should be
804 compared rigorously, but rather as general trends that are expected to hold broadly true.

805 Several examples of strongly fluorescing particles of specific importance to the built
806 environment (e.g. cellulose fibers, particles from cotton t-shirts, and laboratory wipes) show that
807 these particle types could be very important sources of fluorescent particles indoors (i.e. Figs.
808 S4S and S4T). This will also require further study, but should be taken seriously by researchers
809 who utilize UV-LIF instrumentation to estimate concentrations and properties of biological
810 material within homes, indoor occupational environments, or hospitals.



811 The study presented here is meant broadly to achieve two aims. The first aim is to present a
812 summary of fluorescent properties of the most important particle types expected in a given
813 sample and to suggest thresholding strategies (i.e. $FT + 9\sigma$) that may be widely useful for
814 improving analysis quality. The second aim is to suggest key analysis and plotting strategies that
815 other UV-LIF, especially WIBS, instrumentation users can utilize to interrogate particles using
816 their own instruments. By proposing several analysis strategies we aim to introduce concepts to
817 the broader atmospheric community in order to promote deeper discussions about how best to
818 continue improving UV-LIF instrumentation and analyses.

819 6. Acknowledgments

820 The authors acknowledge the University of Denver for financial support from the faculty start-up
821 fund. Nicole Savage acknowledges financial support from the Phillipson Graduate Fellowship at
822 the University of Denver. Christine Krentz acknowledges financial support from the Summer
823 Undergraduate Research Grant program through the Undergraduate Research Center at the
824 University of Denver. Tobias Könemann and Christopher Pöhlker acknowledge financial support
825 by the Max Planck Society and the Max Planck Graduate Center with the Johannes Gutenberg-
826 Universität Mainz (MPGC). Gediminas Mainelis acknowledges support by the New Jersey
827 Agricultural Experiment Station (NJAES) at Rutgers, The State University of New Jersey. Ulrich
828 Pöschl and Meinrat O. Andreae are acknowledged for useful discussions and support for the
829 authors. Gavin McMeeking from Handix Scientific is acknowledged for the development of the
830 WIBS analysis toolkit. Martin Gallagher, Jonathan Crosier, and the Department of Geology and
831 Earth Science in the School of Earth and Environmental Sciences, University of Manchester
832 provided several samples of raw materials. Marie Gosselin is acknowledged for discussions
833 about WIBS analysis, and Ben Swanson is acknowledged for help with the conceptual design of
834 figures.



835 **7. References**

- 836 Abdel-Shafy, H. I., and Mansour, M. S. M.: A review on polycyclic aromatic hydrocarbons:
837 Source, environmental impact, effect on human health and remediation, *Egyptian Journal of*
838 *Petroleum*, 25, 107-123, <http://dx.doi.org/10.1016/j.ejpe.2015.03.011>, 2016.
- 839 Agranovski, V., Ristovski, Z., Hargreaves, M., Blackall, P. J., and Morawska, L.: Real-time
840 measurement of bacterial aerosols with the UVAPS: performance evaluation, *Journal of Aerosol*
841 *Science*, 34, 301-317, 10.1016/s0021-8502(02)00181-7, 2003.
- 842 Agranovski, V., Ristovski, Z. D., Ayoko, G. A., and Morawska, L.: Performance evaluation of
843 the UVAPS in measuring biological aerosols: Fluorescence spectra from NAD(P)H coenzymes
844 and riboflavin, *Aerosol Sci. Technol.*, 38, 354-364, 10.1080/02786820490437505, 2004.
- 845 Aizawa, T., and Kosaka, H.: Investigation of early soot formation process in a diesel spray flame
846 via excitation-emission matrix using a multi-wavelength laser source, *International Journal of*
847 *Engine Research*, 9, 79-96, 10.1243/14680874jer01407, 2008.
- 848 Aizawa, T., and Kosaka, H.: Effects of Fischer-Tropsch diesel fuel on soot formation processes
849 in a diesel spray flame, *International Journal of Engine Research*, 11, 79-87,
850 10.1243/14680874jer04709, 2010.
- 851 Amann, R. I., Ludwig, W., and Schleifer, K. H.: Phylogenetic identification and in-situ
852 detection of individual microbial-cells without cultivation, *Microbiol. Rev.*, 59, 143-169, 1995.
- 853 Ariya, P. A., Sun, J., Eltouny, N. A., Hudson, E. D., and Hayes, C. T.: Physical and chemical
854 characterization of bioaerosols implications for nucleation processes, *Int. Rev. Phys. Chem.*, 28,
855 1-32, 2009.
- 856 Bhangar, S., Huffman, J. A., and Nazaroff, W. W.: Size-resolved fluorescent biological aerosol
857 particle concentrations and occupant emissions in a university classroom, *Indoor Air*, 24, 604-
858 617, 10.1111/ina.12111, 2014.
- 859 Bhangar, S., Adams, R. I., Pasut, W., Huffman, J. A., Arens, E. A., Taylor, J. W., Bruns, T. D.,
860 and Nazaroff, W. W.: Chamber bioaerosol study: human emissions of size-resolved fluorescent
861 biological aerosol particles, *Indoor Air*, 26, 193-206, 10.1111/ina.12195, 2016.
- 862 Brosseau, L. M., Vesley, D., Rice, N., Goodell, K., Nellis, M., and Hairston, P.: Differences in
863 detected fluorescence among several bacterial species measured with a direct-reading particle
864 sizer and fluorescence detector, *Aerosol Sci. Technol.*, 32, 545-558, 2000.
- 865 Chi, M. C., and Li, C. S.: Fluorochrome in monitoring atmospheric bioaerosols and correlations
866 with meteorological factors and air pollutants, *Aerosol Sci. Tech.*, 41, 672-678, 2007.
- 867 Cox, C. S., and Wathes, C. M.: *Bioaerosols Handbook*, Book, Whole, CRC Press, 1995.
- 868 Crawford, I., Lloyd, G., Herrmann, E., Hoyle, C. R., Bower, K. N., Connolly, P. J., Flynn, M. J.,
869 Kaye, P. H., Choularton, T. W., and Gallagher, M. W.: Observations of fluorescent aerosol-cloud



- 870 interactions in the free troposphere at the High-Altitude Research Station Jungfraujoch,
871 Atmospheric Chemistry and Physics, 16, 2273-2284, 10.5194/acp-16-2273-2016, 2016.
- 872 DeCarlo, P. F., Slowik, J. G., Worsnop, D. R., Davidovits, P., and Jimenez, J. L.: Particle
873 morphology and density characterization by combined mobility and aerodynamic diameter
874 measurements. Part 1: Theory, Aerosol Science and Technology, 38, 1185-1205,
875 10.1080/027868290903907, 2004.
- 876 Delort, A. M., Vaitilingom, M., Amato, P., Sancelme, M., and Parazols, M.: A short overview of
877 the microbial population in clouds: potential roles in atmospheric chemistry and nucleation
878 processes, Atmos. Res., 98, 249-260, 2010.
- 879 Després, V. R., Huffman, J. A., Burrows, S. M., Hoose, C., Safatov, A. S., Buryak, G.,
880 Froehlich-Nowoisky, J., Elbert, W., Andreae, M. O., Poeschl, U., and Jaenicke, R.: Primary
881 biological aerosol particles in the atmosphere: a review, Tellus Series B-Chemical and Physical
882 Meteorology, 64, 15598-15598, 10.3402/tellusb.v64i0.15598, 2012.
- 883 Douwes, J., Thorne, P., Pearce, N., and Heederik, D.: Bioaerosol health effects and exposure
884 assessment: Progress and prospects, Annals of Occupational Hygiene, 47, 187-200,
885 10.1093/annhyg/meg032, 2003.
- 886 Finlayson-Pitts, B. J., and Pitts, J., James N.: Chemistry of the Upper and Lower Atmosphere :
887 Theory, Experiments, and Applications (1), Academic Pres, San Diego, USA, 993 pp.,
888 November 1999.
- 889 Fröhlich -Nowoisky, J., Kampf, C. J., Weber, B., Huffman, J. A., Pöhlker, C., Andreae, M. O.,
890 Lang-Yona, N., Burrows, S. M., Gunthe, S. S., Elbert, W., Su, H., Hoor, P., Thines, E.,
891 Hoffmann, T., Despres, V. R., and Poeschl, U.: Bioaerosols in the Earth system: Climate, health,
892 and ecosystem interactions, Atmospheric Research, 182, 346-376,
893 10.1016/j.atmosres.2016.07.018, 2016.
- 894 Gabey, A. M., Gallagher, M. W., Whitehead, J., Dorsey, J. R., Kaye, P. H., and Stanley, W. R.:
895 Measurements and comparison of primary biological aerosol above and below a tropical forest
896 canopy using a dual channel fluorescence spectrometer, Atmospheric Chemistry and Physics, 10,
897 4453-4466, 10.5194/acp-10-4453-2010, 2010.
- 898 Gabey, A. M., Vaitilingom, M., Freney, E., Boulon, J., Sellegri, K., Gallagher, M. W., Crawford,
899 I. P., Robinson, N. H., Stanley, W. R., and Kaye, P. H.: Observations of fluorescent and
900 biological aerosol at a high-altitude site in central France, Atmospheric Chemistry and Physics,
901 13, 7415-7428, 10.5194/acp-13-7415-2013, 2013.
- 902 Gosselin, M. I., Rathnayake, C. M., Crawford, I., Pöhlker, C., Frohlich-Nowoisky, J., Schmer,
903 B., Despres, V. R., Engling, G., Gallagher, M., Stone, E., Pöschl, U., and Huffman, J. A.:
904 Fluorescent bioaerosol particle, molecular tracer, and fungal spore concentrations during dry and
905 rainy periods in a semi-arid forest, Atmospheric Chemistry and Physics, 16, 15165-15184,
906 10.5194/acp-16-15165-2016, 2016.



- 907 Griffiths, W. D., and Decosemo, G. A. L.: THE ASSESSMENT OF BIOAEROSOLS - A
908 CRITICAL-REVIEW, *Journal of Aerosol Science*, 25, 1425-1458, 10.1016/0021-
909 8502(94)90218-6, 1994.
- 910 Hairston, P. P., Ho, J., and Quant, F. R.: Design of an instrument for real-time detection of
911 bioaerosols using simultaneous measurement of particle aerodynamic size and intrinsic
912 fluorescence, *Journal of Aerosol Science*, 28, 471-482, 1997.
- 913 Han, T., Zhen, H. J., Fennell, D. E., and Mainelis, G.: Design and Evaluation of the Field-
914 Deployable Electrostatic Precipitator with Superhydrophobic Surface (FDEPSS) with High
915 Concentration Rate, *Aerosol and Air Quality Research*, 15, 2397-2408,
916 10.4209/aaqr.2015.04.0206, 2015.
- 917 Handorean, A., Robertson, C. E., Harris, J. K., Frank, D., Hull, N., Kotter, C., Stevens, M. J.,
918 Baumgardner, D., Pace, N. R., and Hernandez, M.: Microbial aerosol liberation from soiled
919 textiles isolated during routine residuals handling in a modern health care setting, *Microbiome*, 3,
920 72-72, 10.1186/s40168-015-0132-3, 2015.
- 921 Healy, D. A., Huffman, J. A., O'Connor, D. J., Pohlker, C., Poschl, U., and Sodeau, J. R.:
922 Ambient measurements of biological aerosol particles near Killarney, Ireland: a comparison
923 between real-time fluorescence and microscopy techniques, *Atmospheric Chemistry and Physics*,
924 14, 8055-8069, 10.5194/acp-14-8055-2014, 2014.
- 925 Heidelberg, J. F., Shahamat, M., Levin, M., Rahman, I., Stelma, G., Grim, C., and and Colwell,
926 R. R.: Effect of aerosolization on culturability and viability of gram-negative bacteria, *Appl.*
927 *Environ.*, 63, 3585-3588, 1997.
- 928 Hernandez, M., Perring, A. E., McCabe, K., Kok, G., Granger, G., and Baumgardner, D.:
929 Chamber catalogues of optical and fluorescent signatures distinguish bioaerosol classes,
930 *Atmospheric Measurement Techniques*, 9, 3283-3292, 10.5194/amt-9-3283-2016, 2016.
- 931 Hill, S. C., Pinnick, R. G., Niles, S., Pan, Y. L., Holler, S., Chang, R. K., Bottiger, J., Chen, B.
932 T., Orr, C. S., and and Feather, G.: Real-time measurement of fluorescence spectra from single
933 airborne biological particles, *Field Anal. Chem. Technol.*, 3, 221-239, 1999a.
- 934 Hill, S. C., Pinnick, R. G., Niles, S., Pan, Y. L., Holler, S., Chang, R. K., Bottiger, J., Chen, B.
935 T., Orr, C. S., and Feather, G.: Real-time measurement of fluorescence spectra from single
936 airborne biological particles, *Field Anal. Chem. Technol.*, 3, 221-239, 1999b.
- 937 Hill, S. C., Pinnick, R. G., Niles, S., Fell, N. F., Pan, Y. L., Bottiger, J., Bronk, B. V., Holler, S.,
938 and Chang, R. K.: Fluorescence from Airborne Microparticles: Dependence on Size,
939 Concentration of Fluorophores, and Illumination Intensity, *Appl. Optics*, 40, 3005-3013, 2001.
- 940 Hill, S. C., Williamson, C. C., Doughty, D. C., Pan, Y. L., Santarpia, J. L., and Hill, H. H.: Size-
941 dependent fluorescence of bioaerosols: Mathematical model using fluorescing and absorbing
942 molecules in bacteria, *Journal of Quantitative Spectroscopy & Radiative Transfer*, 157, 54-70,
943 10.1016/j.jqsrt.2015.01.011, 2015.



- 944 Ho, J., Spence, M., and Hairston, P.: Measurement of Biological Aerosol with a Fluorescent
945 Aerodynamic Particle Sizer (FLAPS): Correlation of Optical Data with Biological Data.
946 *Aerobiologia*, 1999.
- 947 Ho, J.: Future of biological aerosol detection, *Advances in Biodetection*, 457, 125-148,
948 [http://dx.doi.org/10.1016/S0003-2670\(01\)01592-6](http://dx.doi.org/10.1016/S0003-2670(01)01592-6), 2002.
- 949 Huffman, J. A., Treutlein, B., and Poeschl, U.: Fluorescent biological aerosol particle
950 concentrations and size distributions measured with an Ultraviolet Aerodynamic Particle Sizer
951 (UV-APS) in Central Europe, *Atmospheric Chemistry and Physics*, 10, 3215-3233, 2010.
- 952 Huffman, J. A., Sinha, B., Garland, R. M., Snee-Pollmann, A., Gunthe, S. S., Artaxo, P., Martin,
953 S. T., Andreae, M. O., and Poschl, U.: Size distributions and temporal variations of biological
954 aerosol particles in the Amazon rainforest characterized by microscopy and real-time UV-APS
955 fluorescence techniques during AMAZE-08, *Atmospheric Chemistry and Physics*, 12, 11997-
956 12019, 10.5194/acp-12-11997-2012, 2012.
- 957 Huffman, J. A., Prenni, A. J., DeMott, P. J., Pohlker, C., Mason, R. H., Robinson, N. H.,
958 Frohlich-Nowoisky, J., Tobo, Y., Despres, V. R., Garcia, E., Gochis, D. J., Harris, E., Mueller-
959 Germann, I., Ruzene, C., Schmer, B., Sinha, B., Day, D. A., Andreae, M. O., Jimenez, J. L.,
960 Gallagher, M., Kreidenweis, S. M., Bertram, A. K., and Poschl, U.: High concentrations of
961 biological aerosol particles and ice nuclei during and after rain, *Atmospheric Chemistry and
962 Physics*, 13, 6151-6164, 10.5194/acp-13-6151-2013, 2013.
- 963 Huffman, J. A., and Santarpia, J. L.: Online techniques for quantification and characterization of
964 biological aerosol, in: *Microbiology of Aerosols*, edited by: Delort, A. M., and Amato, P., Wiley
965 (In Press), Hoboken, NJ, Chapter 4, 2017.
- 966 Jaenicke, R.: Abundance of cellular material and proteins in the atmosphere, *Science*, 308, 73,
967 2005.
- 968 Kaye, P., Aptowicz, K., Chang, R., Foot, V., and Videen, G.: Optics of Biological Particles. In:
969 *Angularly Resolved Elastic Scattering from Airborne Particles*, 2007.
- 970 Kaye, P. H., Eyles, N. A., Ludlow, I. K., and Clark, J. M.: AN INSTRUMENT FOR THE
971 CLASSIFICATION OF AIRBORNE PARTICLES ON THE BASIS OF SIZE, SHAPE, AND
972 COUNT FREQUENCY, *Atmospheric Environment Part a-General Topics*, 25, 645-654,
973 10.1016/0960-1686(91)90062-c, 1991.
- 974 Kaye, P. H., Stanley, W. R., Hirst, E., Foot, E. V., Baxter, K. L., and Barrington, S. J.: Single
975 particle multichannel bio-aerosol fluorescence sensor, *Optics Express*, 13, 3583-3593,
976 10.1364/opex.13.003583, 2005.
- 977 Könemann, T., Savage, N., McMeeking, G., Su, H., Huffman, J. A., Pöhlker, C., and Pöschl, U.:
978 Spectral Intensity Bioaerosol Sensor (SIBS): Technical Description and Laboratory Assessment
979 of a Novel Instrument for Single Particle Detection. In Prep.



- 980 Lavoie, J., Marchand, G. E., Cloutier, Y., Halle, S., Nadeau, S., Duchaine, C., and Pichette, G.:
981 Evaluation of bioaerosol exposures during hospital bronchoscopy examinations, *Environmental*
982 *Science-Processes & Impacts*, 17, 288-299, 10.1039/c4em00359d, 2015.
- 983 Li, J., Zhou, L., Zhang, X., Xu, C., Dong, L., and Yao, M.: Bioaerosol emissions and detection of
984 airborne antibiotic resistance genes from a wastewater treatment plant, *Atmospheric*
985 *Environment*, 124, 404-412, 10.1016/j.atmosenv.2015.06.030, 2016.
- 986 Lv, Y., Li, X., Xu, T. T., Cheng, T. T., Yang, X., Chen, J. M., Iinuma, Y., and Herrmann, H.:
987 Size distributions of polycyclic aromatic hydrocarbons in urban atmosphere: sorption mechanism
988 and source contributions to respiratory deposition, *Atmospheric Chemistry and Physics*, 16,
989 2971-2983, 10.5194/acp-16-2971-2016, 2016.
- 990 Mainelis, G., Berry, D., An, H. R., Yao, M. S., DeVoe, K., Fennell, D. E., and Jaeger, R.: Design
991 and performance of a single-pass bubbling bioaerosol generator, *Atmospheric Environment*, 39,
992 3521-3533, 10.1016/j.atmosenv.2005.02.043, 2005.
- 993 Mason, R. H., Si, M., Li, J., Chou, C., Dickie, R., Toom-Sauntry, D., Poehlker, C., Yakobi-
994 Hancock, J. D., Ladino, L. A., Jones, K., Leitch, W. R., Schiller, C. L., Abbatt, J. P. D.,
995 Huffman, J. A., and Bertram, A. K.: Ice nucleating particles at a coastal marine boundary layer
996 site: correlations with aerosol type and meteorological conditions, *Atmospheric Chemistry and*
997 *Physics*, 15, 12547-12566, 10.5194/acp-15-12547-2015, 2015.
- 998 Mercier, X., Faccineto, A., and Desgroux, P.: *Cleaner Combustion: Developing Detailed*
999 *Chemical Kinetic Models*, Green Energy and Technology, Springer, London, 2013.
- 1000 Morris, C. E., Georgakopoulos, D. G., and Sands, D. C.: Ice nucleation active bacteria and their
1001 potential role in precipitation, *Journal de Physique IV*, 121, 87-103, 10.1051/jp4:2004121004,
1002 2004.
- 1003 Möhler, O., DeMott, P. J., Vali, G., and Levin, Z.: Microbiology and atmospheric processes: the
1004 role of biological particles in cloud physics, *Biogeosciences*, 4, 1059-1071, 2007.
- 1005 Niessner, R., and Krupp, A.: DETECTION AND CHEMICAL CHARACTERIZATION OF
1006 POLYCYCLIC AROMATIC HYDROCARBON AEROSOLS BY MEANS OF LASER-
1007 INDUCED FLUORESCENCE, *Particle & Particle Systems Characterization*, 8, 23-28,
1008 10.1002/ppsc.19910080106, 1991.
- 1009 O'Connor, D. J., Daly, S. M., and Sodeau, J. R.: On-line monitoring of airborne bioaerosols
1010 released from a composting/green waste site, *Waste Management*, 42, 23-30,
1011 10.1016/j.wasman.2015.04.015, 2015a.
- 1012 O'Connor, D. J., Healy, D. A., and Sodeau, J. R.: A 1-month online monitoring campaign of
1013 ambient fungal spore concentrations in the harbour region of Cork, Ireland, *Aerobiologia*, 31,
1014 295-314, 10.1007/s10453-015-9365-7, 2015b.
- 1015 Pan, Y. L., Holler, S., Chang, R. K., Hill, S. C., Pinnick, R. G., Niles, S., Bottiger, J. R., and
1016 Bronk, B. V.: Real-time detection and characterization of individual flowing airborne biological



- 1017 particles: fluorescence spectra and elastic scattering measurements, *P. Soc. Photo-Opt. Ins.*,
1018 3855, 117-125, 1999.
- 1019 Panne, U., Knoller, A., Kotzick, R., and Niessner, R.: On-line and in-situ detection of polycyclic
1020 aromatic hydrocarbons (PAH) on aerosols via thermodesorption and laser-induced fluorescence
1021 spectroscopy, *Fresenius J. Anal. Chem.*, 366, 408-414, 2000.
- 1022 Penner, J. E.: Carbonaceous Aerosols Influencing Atmospheric Radiation: Black and Organic
1023 Carbon, 35, 1994.
- 1024 Perring, A. E., Schwarz, J. P., Baumgardner, D., Hernandez, M. T., Spracklen, D. V., Heald, C.
1025 L., Gao, R. S., Kok, G., McMeeking, G. R., McQuaid, J. B., and Fahey, D. W.: Airborne
1026 observations of regional variation in fluorescent aerosol across the United States, *Journal of*
1027 *Geophysical Research-Atmospheres*, 120, 1153-1170, 10.1002/2014JD022495, 2015.
- 1028 Pinnick, R. G., Hill, S. C., Nachman, P., Pendleton, J. D., Fernandez, G. L., Mayo, M. W., and
1029 Bruno, J. G.: Fluorescence Particle Counter for Detecting Airborne Bacteria and Other
1030 Biological Particles, *Aerosol Sci. Technol.*, 23, 653-664, 1995.
- 1031 Powelson, M. H., Espelien, B. M., Hawkins, L. N., Galloway, M. M., and De Haan, D. O.:
1032 Brown Carbon Formation by Aqueous-Phase Carbonyl Compound Reactions with Amines and
1033 Ammonium Sulfate, *Environmental Science & Technology*, 48, 985-993, 10.1021/es4038325,
1034 2014.
- 1035 Primmerman, C.: Detection of biological agents. *Lincoln Laboratory Journal*, 2000.
- 1036 Pöhlker, C., Huffman, J. A., and Poeschl, U.: Autofluorescence of atmospheric bioaerosols -
1037 fluorescent biomolecules and potential interferences, *Atmospheric Measurement Techniques*, 5,
1038 37-71, 10.5194/amt-5-37-2012, 2012.
- 1039 Pöhlker, C., Huffman, J. A., Foerster, J. D., and Poeschl, U.: Autofluorescence of atmospheric
1040 bioaerosols: spectral fingerprints and taxonomic trends of pollen, *Atmospheric Measurement*
1041 *Techniques*, 6, 3369-3392, 10.5194/amt-6-3369-2013, 2013.
- 1042 Pöschl, U.: Atmospheric aerosols: Composition, transformation, climate and health effects,
1043 *Angewandte Chemie-International Edition*, 44, 7520-7540, 10.1002/anie.200501122, 2005.
- 1044 Pöschl, U., Martin, S. T., Sinha, B., Chen, Q., Gunthe, S. S., Huffman, J. A., Borrmann, S.,
1045 Farmer, D. K., Garland, R. M., Helas, G., Jimenez, J. L., King, S. M., Manzi, A., Mikhailov, E.,
1046 Pauliquevis, T., Petters, M. D., Prenni, A. J., Roldin, P., Rose, D., Schneider, J., Su, H., Zorn, S.
1047 R., Artaxo, P., and Andreae, M. O.: Rainforest Aerosols as Biogenic Nuclei of Clouds and
1048 Precipitation in the Amazon, *Science*, 329, 1513-1516, 10.1126/science.1191056, 2010.
- 1049 Robinson, E., Gao, R.-S., Schwarz, J., Fahey, D., and Perring, A.: Fluorescence Calibration
1050 Method for Single Particle Aerosol Fluorescence Instruments. 2017.
- 1051 Saari, S., Mensah-Attipoe, J., Reponen, T., Veijalainen, A. M., Salmela, A., Pasanen, P., and
1052 Keskinen, J.: Effects of fungal species, cultivation time, growth substrate, and air exposure



- 1053 velocity on the fluorescence properties of airborne fungal spores, *Indoor Air*, 25, 653-661,
1054 10.1111/ina.12166, 2015a.
- 1055 Saari, S., Niemi, J. V., Ronkko, T., Kuuluvainen, H., Jarvinen, A., Pirjola, L., Aurela, M.,
1056 Hillamo, R., and Keskinen, J.: Seasonal and Diurnal Variations of Fluorescent Bioaerosol
1057 Concentration and Size Distribution in the Urban Environment, *Aerosol and Air Quality
1058 Research*, 15, 572-581, 10.4209/aaqr.2014.10.0258, 2015b.
- 1059 Sivaprakasam, V., Lin, H. B., Huston, A. L., and Eversole, J. D.: Spectral characterization of
1060 biological aerosol particles using two-wavelength excited laser-induced fluorescence and elastic
1061 scattering measurements, *Optics Express*, 19, 6191-6208, 10.1364/oe.19.006191, 2011.
- 1062 Slowik, J. G., Cross, E. S., Han, J. H., Kolucki, J., Davidovits, P., Williams, L. R., Onasch, T. B.,
1063 Jayne, J. T., Kolb, C. E., and Worsnop, D. R.: Measurements of morphology changes of fractal
1064 soot particles using coating and denuding experiments: Implications for optical absorption and
1065 atmospheric lifetime, *Aerosol Science and Technology*, 41, 734-750,
1066 10.1080/02786820701432632, 2007.
- 1067 Sodeau, J. R., and O'Connor, D. J.: Chapter 16 - Bioaerosol Monitoring of the Atmosphere for
1068 Occupational and Environmental Purposes, in: *Comprehensive Analytical Chemistry, The
1069 Quality of Air*, Elsevier, 391-420, 2016.
- 1070 Taketani, F., Kanaya, Y., Nakamura, T., Koizumi, K., Moteki, N., and Takegawa, N.:
1071 Measurement of fluorescence spectra from atmospheric single submicron particle using laser-
1072 induced fluorescence technique, *Journal of Aerosol Science*, 58, 1-8,
1073 10.1016/j.jaerosci.2012.12.002, 2013.
- 1074 Toprak, E., and Schnaiter, M.: Fluorescent biological aerosol particles measured with the
1075 Waveband Integrated Bioaerosol Sensor WIBS-4: laboratory tests combined with a one year
1076 field study, *Atmospheric Chemistry and Physics*, 13, 225-243, 10.5194/acp-13-225-2013, 2013.
- 1077 Twohy, C. H., McMeeking, G. R., DeMott, P. J., McCluskey, C. S., Hill, T. C. J., Burrows, S.
1078 M., Kulkarni, G. R., Tanarhte, M., Kafle, D. N., and Toohey, D. W.: Abundance of fluorescent
1079 biological aerosol particles at temperatures conducive to the formation of mixed-phase and cirrus
1080 clouds, *Atmospheric Chemistry and Physics*, 16, 8205-8225, 10.5194/acp-16-8205-2016, 2016.
- 1081 Valsan, A. E., Ravikrishna, R., Biju, C. V., Poehlker, C., Despres, V. R., Huffman, J. A.,
1082 Poeschl, U., and Gunthe, S. S.: Fluorescent biological aerosol particle measurements at a tropical
1083 high-altitude site in southern India during the southwest monsoon season, *Atmospheric
1084 Chemistry and Physics*, 16, 9805-9830, 10.5194/acp-16-9805-2016, 2016.
- 1085 Von Helden, G., Hsu, M. T., Gotts, N., and Bowers, M. T.: CARBON CLUSTER CATIONS
1086 WITH UP TO 84 ATOMS - STRUCTURES, FORMATION MECHANISM, AND
1087 REACTIVITY, *Journal of Physical Chemistry*, 97, 8182-8192, 10.1021/j100133a011, 1993.
- 1088 Whitehead, J. D., Gallagher, M. W., Dorsey, J. R., Robinson, N., Gabey, A. M., Coe, H.,
1089 McFiggans, G., Flynn, M. J., Ryder, J., Nemitz, E., and Davies, F.: Aerosol fluxes and dynamics



- 1090 within and above a tropical rainforest in South-East Asia, *Atmospheric Chemistry and Physics*,
1091 10, 9369-9382, 10.5194/acp-10-9369-2010, 2010.
- 1092 Whitehead, J. D., Darbyshire, E., Brito, J., Barbosa, H. M. J., Crawford, I., Stern, R., Gallagher,
1093 M. W., Kaye, P. H., Allan, J. D., Coe, H., Artaxo, P., and McFiggans, G.: Biogenic cloud nuclei
1094 in the central Amazon during the transition from wet to dry season, *Atmospheric Chemistry and*
1095 *Physics*, 16, 9727-9743, 10.5194/acp-16-9727-2016, 2016.
- 1096 Wright, T. P., Hader, J. D., McMeeking, G. R., and Petters, M. D.: High Relative Humidity as a
1097 Trigger for Widespread Release of Ice Nuclei, *Aerosol Science and Technology*, 48, 5,
1098 10.1080/02786826.2014.968244, 2014.
- 1099 Wu, Y., Chen, A. L., Luhung, I., Gall, E. T., Cao, Q. L., Chang, V. W. C., and Nazaroff, W. W.:
1100 Bioaerosol deposition on an air-conditioning cooling coil, *Atmospheric Environment*, 144, 257-
1101 265, 10.1016/j.atmosenv.2016.09.004, 2016.
- 1102 Xie, Y. Y., Fajardo, O. A., Yan, W. Z., Zhao, B., and Jiang, J. K.: Six-day measurement of size-
1103 resolved indoor fluorescent bioaerosols of outdoor origin in an office, *Particuology*, 31, 161-169,
1104 10.1016/j.partic.2016.09.004, 2017.
- 1105 Yu, X. W., Wang, Z. B., Zhang, M. H., Kuhn, U., Xie, Z. Q., Cheng, Y. F., Poschl, U., and Su,
1106 H.: Ambient measurement of fluorescent aerosol particles with a WIBS in the Yangtze River
1107 Delta of China: potential impacts of combustion-related aerosol particles, *Atmospheric*
1108 *Chemistry and Physics*, 16, 11337-11348, 10.5194/acp-16-11337-2016, 2016.
- 1109 Zelenyuk, A., Cai, Y., and Imre, D.: From agglomerates of spheres to irregularly shaped
1110 particles: Determination of dynamic shape factors from measurements of mobility and vacuum
1111 aerodynamic diameters, *Aerosol Science and Technology*, 40, 197-217,
1112 10.1080/02786820500529406, 2006.
- 1113 Zhen, H., Han, T., Fennell, D., and Mainelis, G.: A systematic comparison of four bioaerosol
1114 generators: Effect on culturability and membrane integrity when aerosolizing *E. coli* bacteria.,
1115 *Journal of Aerosol Science*, 2014
- 1116 Ziemba, L. D., Beyersdorf, A. J., Chen, G., Corr, C. A., Crumeyrolle, S. N., Diskin, G., Hudgins,
1117 C., Martin, R., Mikoviny, T., Moore, R., Shook, M., Thornhill, K. L., Winstead, E. L., Wisthaler,
1118 A., and Anderson, B. E.: Airborne observations of bioaerosol over the Southeast United States
1119 using a Wideband Integrated Bioaerosol Sensor, *Journal of Geophysical Research-Atmospheres*,
1120 121, 8506-8524, 10.1002/2015JD024669, 2016.
- 1121
- 1122

1123 **8. Tables**

1124 Table 1. Fluorescence values of standard PSLs, determined as the peak (mean) of a Gaussian fit
1125 applied to a histogram of the fluorescence signal in each channel. Uncertainties are one standard
1126 deviation from the Gaussian mean.

	FL1	FL2	FL3
2 μm Green	69 ± 49	1115 ± 57	214 ± 29
2 μm Red	44 ± 30	160 ± 18	28 ± 13
2.1 μm Blue	724 ± 111	1904 ± 123	2045 ± 6

1127



1128 **Table 2.** Median values for each of the five data parameters, along with percent of particles that
 1129 saturate fluorescence detector in each fluorescence channel. Uncertainty (as one standard
 1130 deviation, σ) listed for particle size and asymmetry factor (AF). Only a sub-selection of pollen
 1131 are characterized as fragmented pollen because not all pollen presented the smaller size fraction
 1132 or fluorescence characteristics that represent fragments.

Materials	FL1	FL1 Sat %	FL2	FL2 Sat %	FL3	FL3 Sat %	Size (μm)	AF	Aerosolization method	
BIOLOGICAL MATERIALS										
Pollen										
Intact Pollen										
1	<i>Urtica dioica</i> (Stinging Nettle)	2047.0	99.2	2047.0	99.4	1072.0	9.9	16.9 \pm 2.2	18.5 \pm 8.3	Powder (P1)
2	<i>Artemisia vulgaris</i> (Common Mugwort)	1980.0	48.3	2047.0	99.7	2047.0	90.3	19.7 \pm 1.0	14.2 \pm 7.6	Powder (P1)
3	<i>Castanea sativa</i> (European Chestnut)	830.0	19.3	258.0	2.9	269.0	0.8	15.3 \pm 1.7	17.0 \pm 9.5	Powder (P1)
4	<i>Corylus avellana</i> (Hazel)	1371.0	44.4	532.0	5.6	99.0	2.8	16.6 \pm 2.1	24.2 \pm 12.6	Powder (P1)
5	<i>Taxus baccata</i> (Common Yew)	525.0	0.4	561.0	0.2	615.0	0.0	16.0 \pm 1.3	22.2 \pm 10.0	Powder (P1)
6	<i>Rumex acetosella</i> (Sheep Sorrel)	2047.0	73.5	2047.0	55.1	693.0	2.7	16.2 \pm 2.0	21.7 \pm 10.8	Powder (P1)
7	<i>Olea europaea</i> (European Olive Tree)	131.0	1.1	395.0	0.4	119.0	0.0	19.7 \pm 1.2	17.7 \pm 7.6	Powder (P1)
8	<i>Alnus glutinosa</i> (Black Alder)	109.0	3.3	432.0	1.2	102.0	0.9	18.6 \pm 1.7	15.8 \pm 8.5	Powder (P1)
9	<i>Phleum pratense</i> (Timothy Grass)	2047.0	100.0	2012.0	49.8	651.0	1.9	15.1 \pm 1.7	24.1 \pm 12.2	Powder (P1)
10	<i>Populus alba</i> (White Poplar)	2047.0	95.9	2047.0	92.2	1723.0	39.2	18.7 \pm 1.9	21.2 \pm 10.4	Powder (P1)
11	<i>Taraxacum officinale</i> (Common Dandelion)	2047.0	99.1	1309.0	21.8	1767.0	44.2	15.4 \pm 1.8	22.2 \pm 11.9	Powder (P1)
12	<i>Amaranthus retroflexus</i> (Redroot Amaranth)	980.0	36.7	1553.0	36.7	1061.0	18.0	17.7 \pm 2.2	19.4 \pm 12.1	Powder (P1)
13	<i>Aesculus hippocastanum</i> (Horse-chestnut)	762.0	23.5	876.0	23.5	776.0	23.5	16.2 \pm 2.0	22.2 \pm 13.4	Powder (P1)
14	<i>Lycopodium</i> (Clubmoss)	40.0	0.1	32.0	0.0	27.0	0.0	3.9 \pm 1.86	24.5 \pm 15.9	Powder (P1)
Fragment Pollen										
3	<i>Castanea sativa</i> (European Chestnut)	74.0	11.0	113.0	0.4	84.0	0.1	7.0 \pm 3.1	24.6 \pm 13.7	Powder (P1)
4	<i>Corylus avellana</i> (Hazel)	263.0	28.8	119.0	0.5	46.0	0.2	6.1 \pm 3.7	20.4 \pm 13.7	Powder (P1)
5	<i>Taxus baccata</i> (Common Yew)	40.0	0.2	28.0	0.1	34.0	0.0	2.6 \pm 2.2	16.0 \pm 12.2	Powder (P1)
6	<i>Rumex acetosella</i> (Sheep Sorrel)	417.0	87.1	88.0	0.4	71.0	0.1	6.0 \pm 2.5	24.4 \pm 12.4	Powder (P1)
7	<i>Olea europaea</i> (European Olive Tree)	40.0	1.9	22.0	0.1	33.0	0.0	2.6 \pm 1.6	10.4 \pm 9.3	Powder (P1)
8	<i>Alnus glutinosa</i> (Black Alder)	46.0	4.6	46.0	0.3	44.0	0.2	6.1 \pm 3.2	25.2 \pm 14.6	Powder (P1)
9	<i>Phleum pratense</i> (Timothy Grass)	2047.0	85.5	129.0	1.2	63.0	0.1	6.0 \pm 3.2	23.1 \pm 13.4	Powder (P1)
10	<i>Populus alba</i> (White Poplar)	642.0	35.2	237.0	8.6	103.0	0.5	7.4 \pm 4.0	24.7 \pm 14.2	Powder (P1)
11	<i>Taraxacum officinale</i> (Common Dandelion)	2047.0	71.9	195.0	0.4	88.0	0.8	6.1 \pm 3.1	23.7 \pm 13.5	Powder (P1)



12	<i>Amaranthus retroflexus</i> (Redroot Amaranth)	104.0	15.6	138.0	5.6	101.0	3.4	7.3 ± 2.8	27.7 ± 14.6	Powder (P1)
13	<i>Aesculus hippocastanum</i> (Horse-chestnut)	43.0	6.0	106.0	0.2	42.0	0.2	4.3 ± 3.1	19.7 ± 13.4	Powder (P1)
Fungal spores										
1	<i>Aspergillus brasiliensis</i>	1279.0	38.5	22.0	0.0	33.0	0.0	3.6 ± 1.8	20.8 ± 10.3	Fungal
2	<i>Aspergillus niger</i> ; WB 326	543.0	6.2	18.0	0.0	29.0	0.0	2.7 ± 0.9	17.1 ± 10.7	Fungal
3	<i>Rhizopus stolonifera</i> (Black Bread Mold); UNB-1	78.0	11.2	20.0	0.1	34.0	0.1	4.4 ± 2.3	21.4 ± 14.4	Fungal
4	<i>Saccharomyces cerevisiae</i> (Brewer's Yeast)	2047.0	96.6	97.0	0.3	41.0	0.1	7.2 ± 3.7	28.7 ± 16.8	Fungal
5	<i>Aspergillus versicolor</i> ; NRRL 238	2047.0	78.2	55.0	0.0	40.0	0.0	4.5 ± 2.5	24.5 ± 16.9	Fungal
Bacteria										
1	<i>Bacillus atrophaeus</i>	443.0	1.0	10.0	0.0	36.0	0.0	2.2 ± 0.4	17.4 ± 4.1	Bacterial
2	<i>Escherichia coli</i>	454.0	1.4	12.0	0.0	33.0	0.0	1.2 ± 0.3	19.3 ± 2.8	Bacterial
3	<i>Pseudomonas Stutzeri</i>	675.0	0.4	16.0	0.0	36.0	0.0	1.1 ± 0.3	19.2 ± 2.8	Bacterial
Biofluorophores										
1	Riboflavin	41.0	0.0	190.0	2.5	119.0	1.3	2.5 ± 2.5	13.2 ± 12.2	Powder (P1)
2	Chitin	116.5	6.2	61.0	0.1	40.0	0.0	2.7 ± 2.1	16.1 ± 13.5	Powder (P1)
3	NAD	49.0	0.2	962.0	26.7	515.0	15.0	2.1 ± 2.2	12.2 ± 10.1	Powder (P1)
4	Folic Acid	41.0	0.0	34.0	0.1	28.0	0.1	3.7 ± 3.4	18.6 ± 13.6	Powder (P1)
5	Cellulose, fibrous medium	54.0	0.2	37.0	0.1	27.0	0.0	3.7 ± 2.5	20.4 ± 15.7	Powder (P1)
6	Ergosterol	2047.0	81.8	457.0	2.6	355.0	11.6	6.8 ± 4.0	22.6 ± 12.9	Powder (P1)
7	Pyridoxine	661.0		39.0		28.0		1.0 ± 0.2	20.0 ± 13.0	Powder (P1)
8	Pyridoxamine	706.0	10.7	40.0	0.0	28.0	0.0	5.2 ± 2.5	20.2 ± 12.7	Powder (P1)
9	Tyrosine	2047.0	59.7	42.0	0.0	29.0	0.0	2.9 ± 3.4	15.4 ± 11.6	Powder (P1)
10	Phenylalanine	53.0	0.0	29.0	0.0	24.0	0.0	3.2 ± 2.0	21.1 ± 15.4	Powder (P1)
11	Tryptophan	2047.0	78.0	357.0	9.0	30.0	0.0	3.5 ± 2.9	20.9 ± 17.0	Powder (P1)
12	Histidine	59.0	0.2	29.0	0.0	25.0	0.0	2.0 ± 1.7	11.6 ± 10.0	Powder (P1)
NON-BIOLOGICAL MATERIALS										
Dust										
1	Arabic Sand	48.0	0.1	37.0	0.0	29.0	0.0	3.1 ± 2.2	16.1 ± 15.7	Powder (P3)
2	California Sand	66.0	1.1	42.0	0.0	31.0	0.0	4.0v1.9	18.8 ± 14.6	Powder (P2)
3	Africa Sand	88.0	0.0	48.0	0.0	26.0	0.0	2.2 ± 1.4	15.3 ± 11.0	Powder (P2)
4	Murkee-Murkee Australian Sand	88.0	0.7	47.0	0.0	26.0	0.0	1.9 ± 1.1	10.9 ± 9.2	Powder (P2)



5	Manua Key Summit Hawaii Sand	54.0	0.1	33.0	0.0	25.0	0.0	1.5 ± 0.7	10.8 ± 13.4	Powder (P2)
6	Quartz	66.0	0.0	38.0	0.0	24.0	0.0	1.7 ± 0.8	11.2 ± 12.7	Powder (P2)
7	Kakadu Dust	58.0	0.0	35.0	0.0	25.0	0.0	2.7 ± 1.4	15.0 ± 12.0	Powder (P2)
8	Feldspar	60.0	0.0	36.0	0.0	25.0	0.0	1.2 ± 0.6	10.2 ± 10.6	Powder (P2)
9	Hematite	51.0	0.0	32.0	0.0	25.0	0.0	1.8 ± 1.0	10.8 ± 11.9	Powder (P2)
10	Gypsum	49.0	0.0	30.0	0.0	26.0	0.0	4.1 ± 3.0	19.3 ± 12.2	Powder (P2)
11	Bani AMMA	48.0	0.2	31.0	0.0	26.0	0.0	3.1 ± 2.1	15.8 ± 13.7	Powder (P2)
12	Arizona Test Dest	46.0	0.0	29.0	0.0	25.0	0.0	1.4 ± 0.7	10.5 ± 10.5	Powder (P2)
13	Kaolinite	46.0	0.0	29.0	0.0	25.0	0.0	1.5 ± 0.8	9.9 ± 10.3	Powder (P2)
HULIS										
1	Waskish Peat Humic Acid Reference	46.0	0.0	29.0	0.0	25.0	0.0	1.7 ± 0.8	10.9 ± 9.8	Powder (P1)
2	Suwannee River Humic Acid Standard II	46.0	0.0	30.0	0.0	26.0	0.0	2.0 ± 1.2	13.2 ± 16.5	Powder (P2)
3	Suwannee River Fulvic Acid Standard I	46.0	0.0	34.0	0.0	28.0	0.0	1.7 ± 1.0	12.0 ± 10.1	Powder (P2)
4	Elliott Soil Humic Acid Standard	47.0	0.0	29.0	0.0	25.0	0.0	1.2 ± 0.6	10.5 ± 10.2	Powder (P1)
5	Pony Lake (Antarctica) Fulvic Acid Reference	46.0	0.0	49.0	0.0	37.0	0.0	2.4 ± 1.8	14.0 ± 13.3	Powder (P2)
6	Nordic Aquatic Fulvic Acid Reference	48.0	0.1	32.0	0.0	27.0	0.0	1.8 ± 1.4	11.6 ± 9.6	Powder (P2)
Polycyclic Hydrocarbons										
1	Pyrene	490.0	7.4	2047.0	91.5	2047.0	81.8	5.0 ± 3.5	17.4 ± 12.6	Powder (P1)
2	Phenanthrene	2047.0	81.9	2047.0	66.3	360.0	22.4	3.9 ± 3.5	14.5 ± 13.6	Powder (P1)
3	Naphthalene	886.0	11.6	45.0	2.1	30.0	0.7	1.1 ± 1.0	10.6 ± 9.5	Powder (P1)
Combustion Soot and Smoke										
1	Aquadag	22.0	0.0	14.0	0.0	29.0	0.0	1.2 ± 0.6	10.5 ± 6.6	Liquid
2	Ash	48.0	0.2	31.0	0.0	23.0	0.0	1.7 ± 1.3	12.6 ± 11.9	Powder (P1)
3	Fullerene Soot	318.0	0.0	30.0	0.0	26.0	0.0	1.1 ± 0.5	17.0 ± 10.6	Powder (P2)
4	Diesel Soot	750.5	0.2	30.0	0.0	26.0	0.0	1.1 ± 0.4	21.2 ± 10.1	Powder (P1)
5	Cigarette Smoke	28.0	0.6	30.0	0.1	36.0	0.0	1.0 ± 0.8	9.5 ± 4.5	Smoke
6	Wood Smoke (<i>Pinus Nigra</i> , <i>Black Pine</i>)	32.0	0.1	30.0	0.0	36.0	0.0	1.0 ± 0.7	9.5 ± 4.3	Smoke
7	Fire Ash	42.0	0.2	33.0	0.0	28.0	0.0	1.8 ± 1.2	14.0 ± 16.7	Powder (P1)
Brown Carbon										
1	Methylglyoxal + Glycine	17.0	0.0	53.0	0.0	88.0	0.0	1.2 ± 0.4	18.4 ± 3.1	Liquid
2	Glycolaldehyde + Methylamine	15.0	0.0	19.0	0.0	47.0	0.0	1.2 ± 0.4	17.9 ± 2.4	Liquid
3	Glyoxal + Ammonium Sulfate	30.0	0.0	9.0	0.0	35.0	0.0	1.3 ± 0.6	14.1 ± 3.5	Liquid

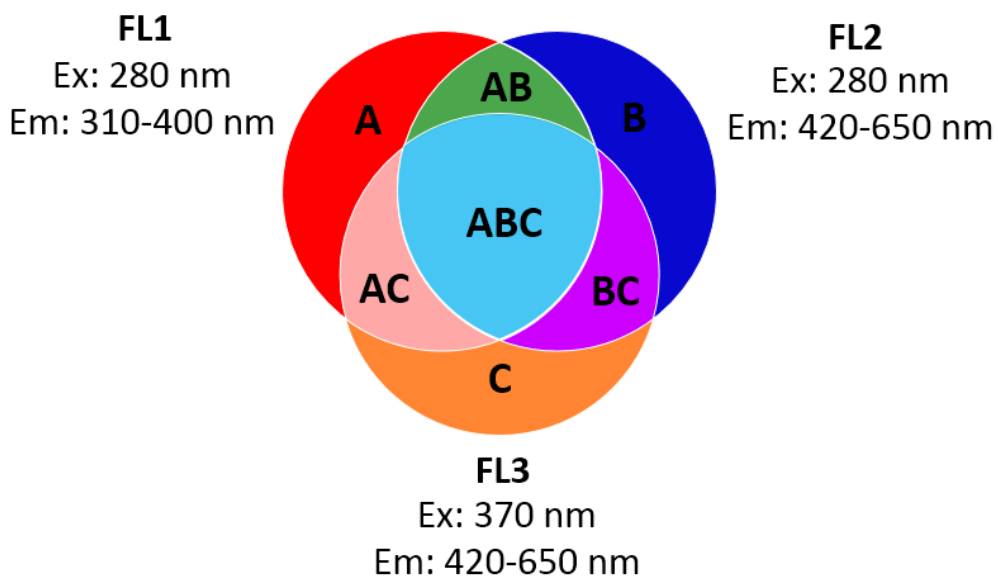


Miscellaneous non-biological										
1	Laboratory wipes	112.0	30.6	54.0	15.2	47.0	15.4	3.6v5.7	16.4 ± 14.4	Rubbed material over inlet
2	Cotton t-shirt (white)	567.0	34.9	145.0	16.1	139.0	16.4	4.9 ± 4.7	23.5 ± 16.2	
3	Cotton t-shirt (black)	56.0	13.5	22.0	1.7	34.0	1.5	2.7 ± 4.0	17.6 ± 14.8	

1133

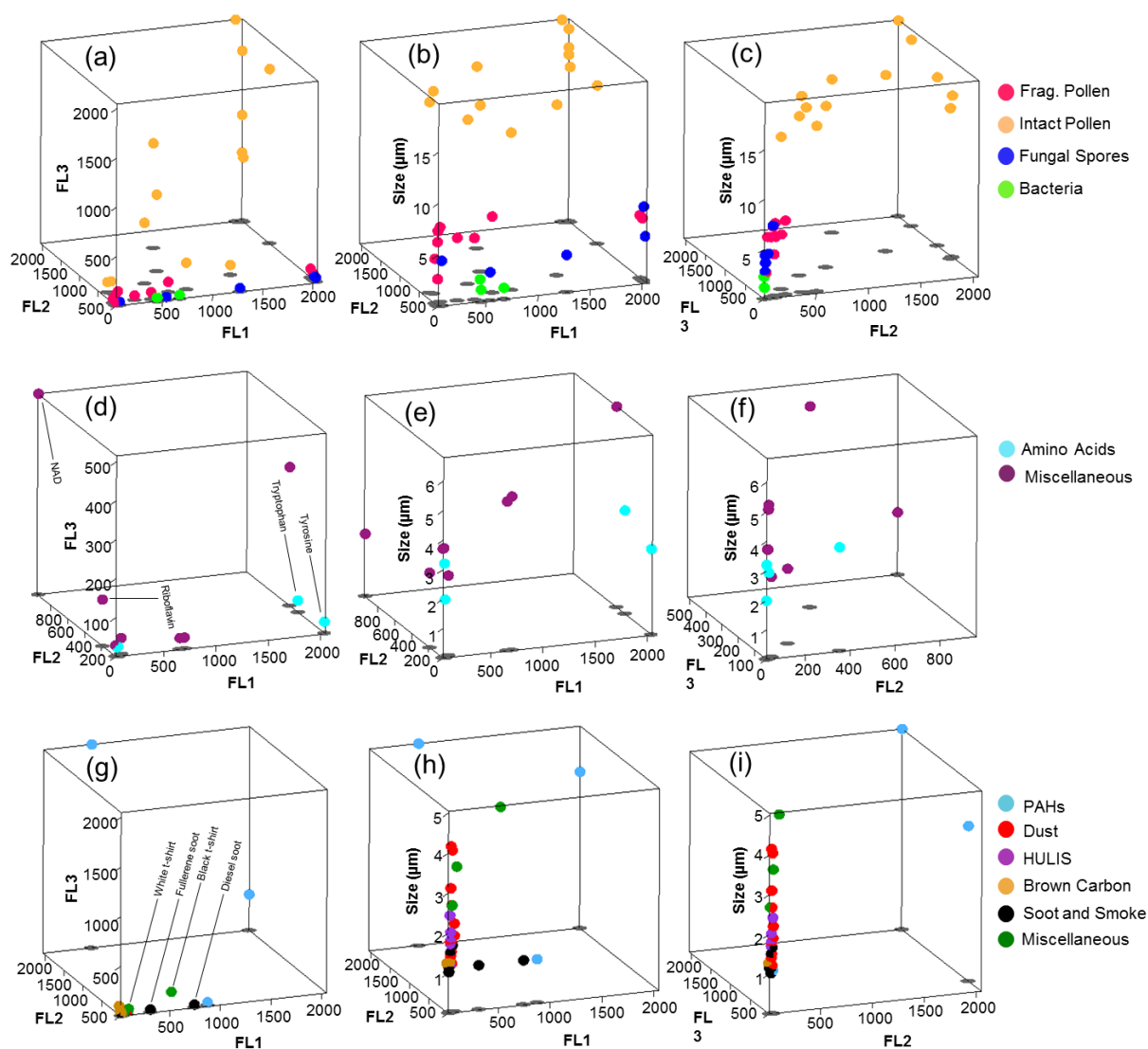


1134 **9. Figures**



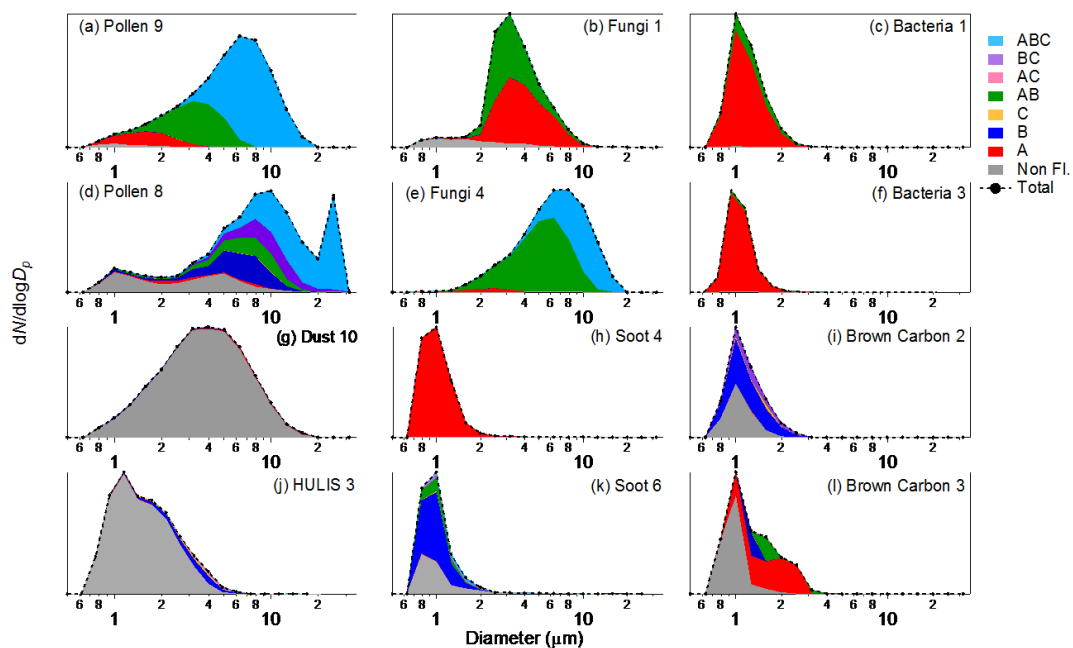
1135

1136 **Figure 1.** Particle type classification, as introduced by introduced by Perring et al. (2015). Large
1137 circles each represent one fluorescence channel (FL1, FL2, FL3). Colored zones represent
1138 particle types that each exhibit fluorescence in one, two, or three channels.



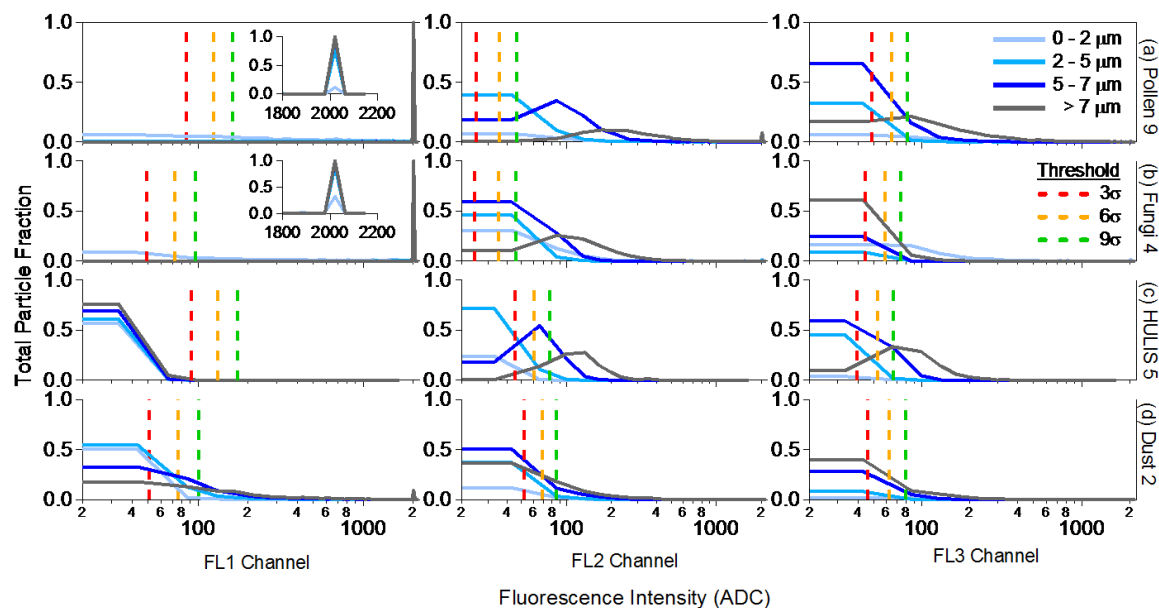
1139

1140 **Figure 2.** Representations including 4 of the 5 parameters recorded by the WIBS: FL1, FL2, FL3,
 1141 and particle size. Biological material types (a-c), bio-fluorophores (d-f), and non-biological
 1142 particle types (g-i). Data points represent median values. Gray ovals are shadows (cast directly
 1143 downward onto the bottom plane) included to help reader with 3-D representation. Tags in (d)
 1144 and (g) used to differentiate particles of specific importance within text.



1145

1146 Figure 3. Stacked particle type size distributions including particle type classification, as
 1147 introduced by introduced by Perring et al. (2015) using FT + 3 σ threshold definition. Examples
 1148 of each material type were selected to show general trends from larger pool of samples. Soot 4
 1149 (h) as an example of combustion soot and Soot 6 (wood smoke) as an example of smoke aerosol.

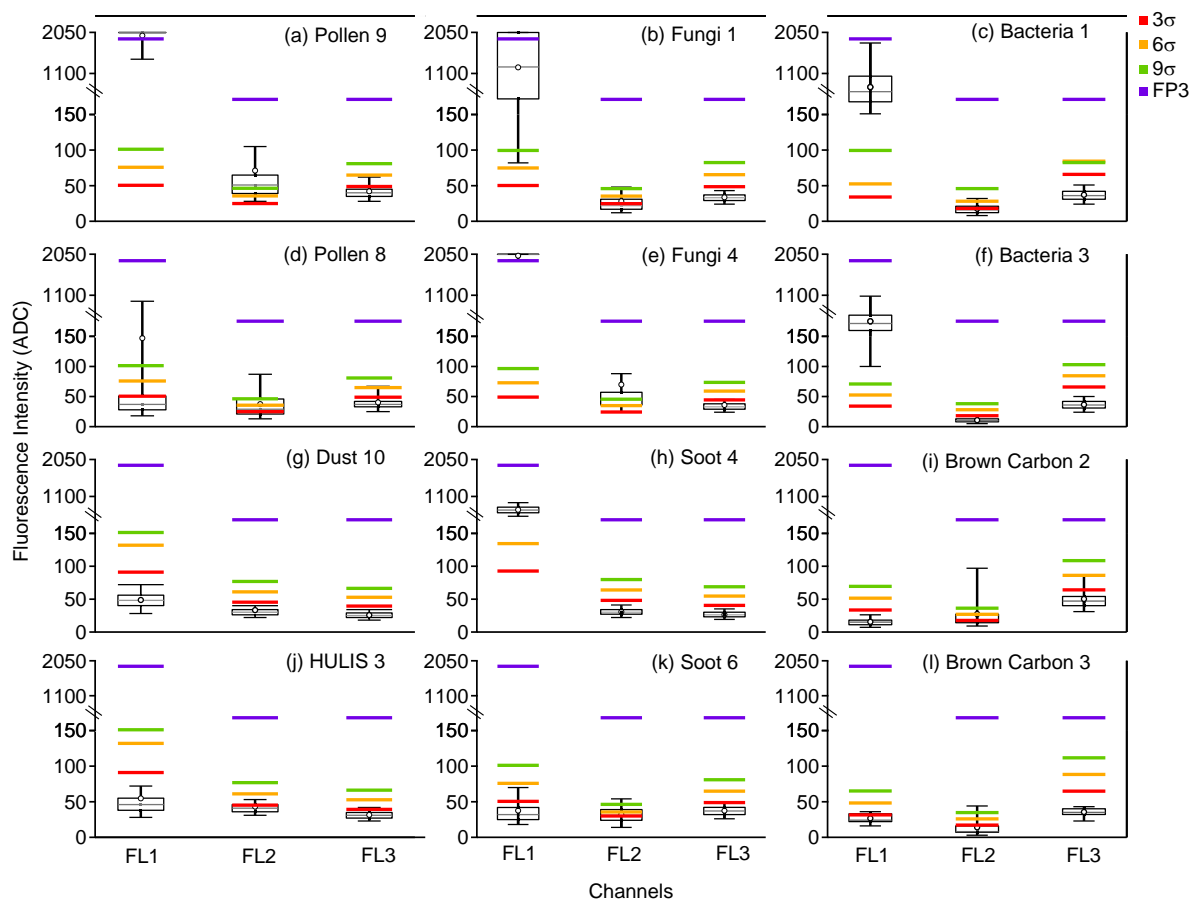


1150

1151

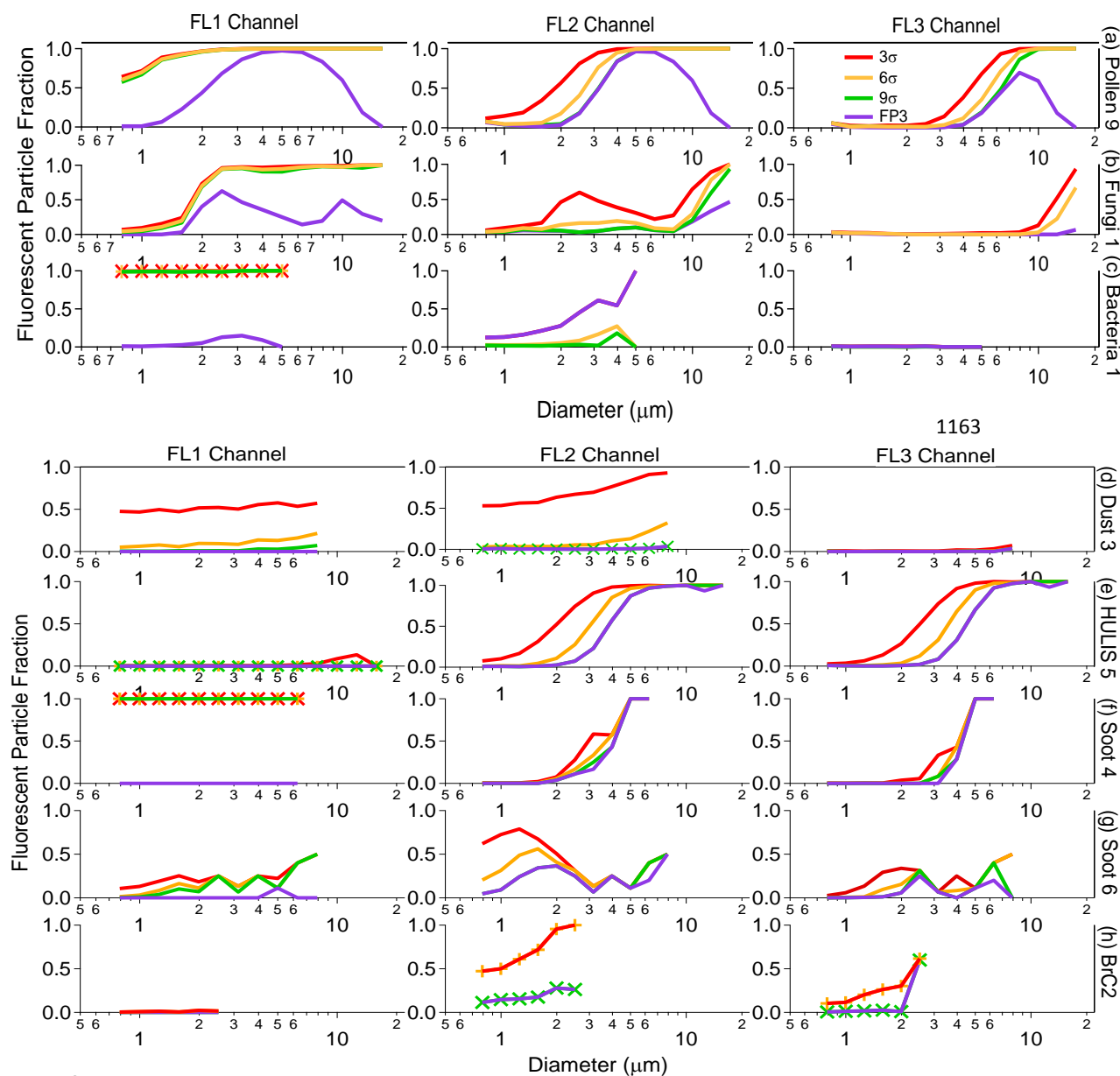
1152 Figure 4. Relative fraction of fluorescent particles versus fluorescence intensity in analog-to-
1153 digital counts (ADC) for each channel. Particles are binned into 4 different size ranges (trace
1154 colors). Vertical lines indicate three thresholding definitions. Insets shown for particles that
1155 exhibit fluorescence saturation characteristics.

1156



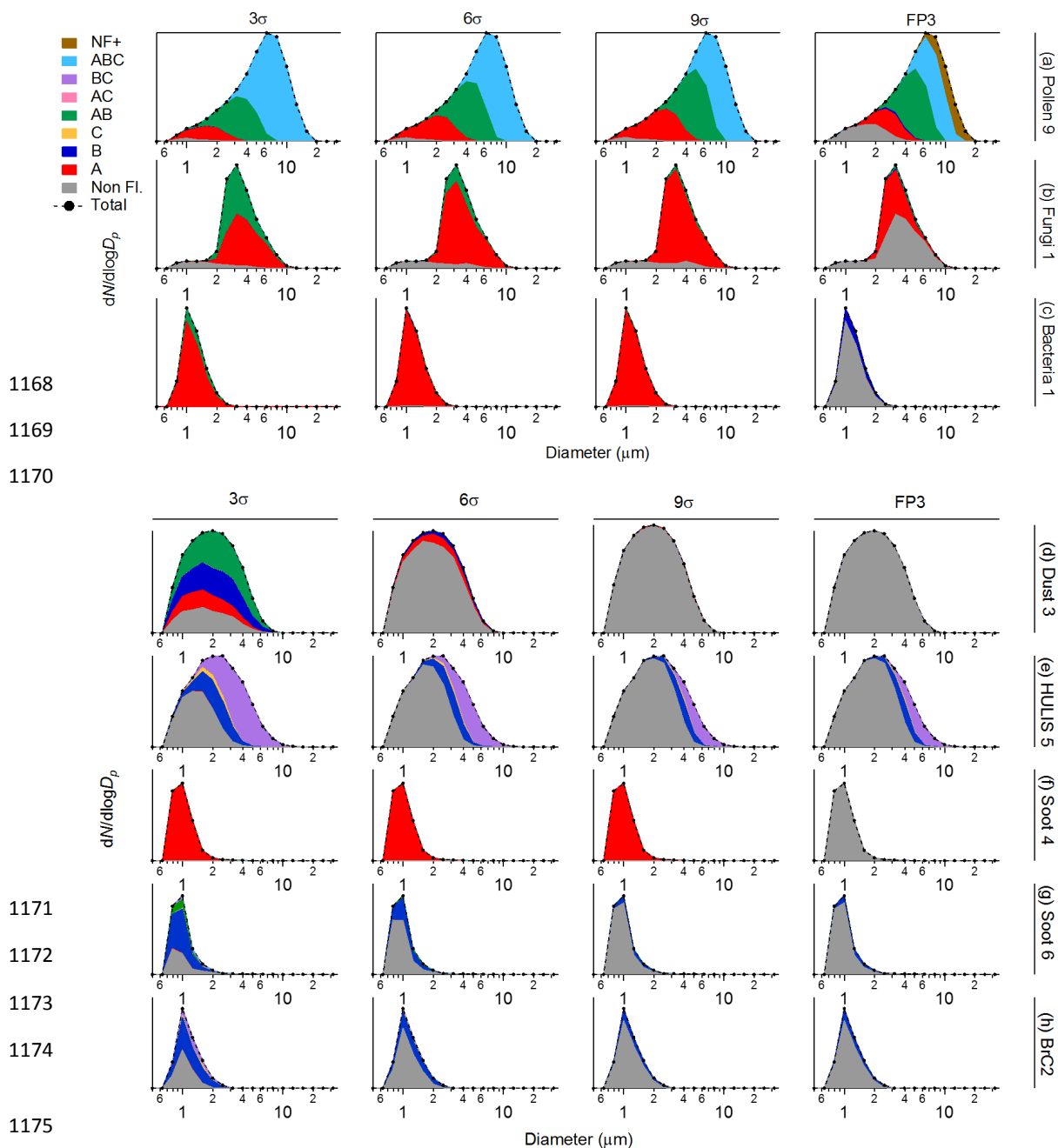
1157

1158 **Figure 5.** Box whisker plots showing statistical distributions of fluorescence intensity in analog-
 1159 to-digital counts (ADC) in each channel. Averages are limited to particles in the size range 3.5-
 1160 4.0 μm for pollen, fungal spore, HULIS, and dust samples and in the range 1.0-1.5 μm for
 1161 bacteria, brown carbon, and soot samples. Horizontal bars associated with each box-whisker
 1162 show four separate threshold levels.

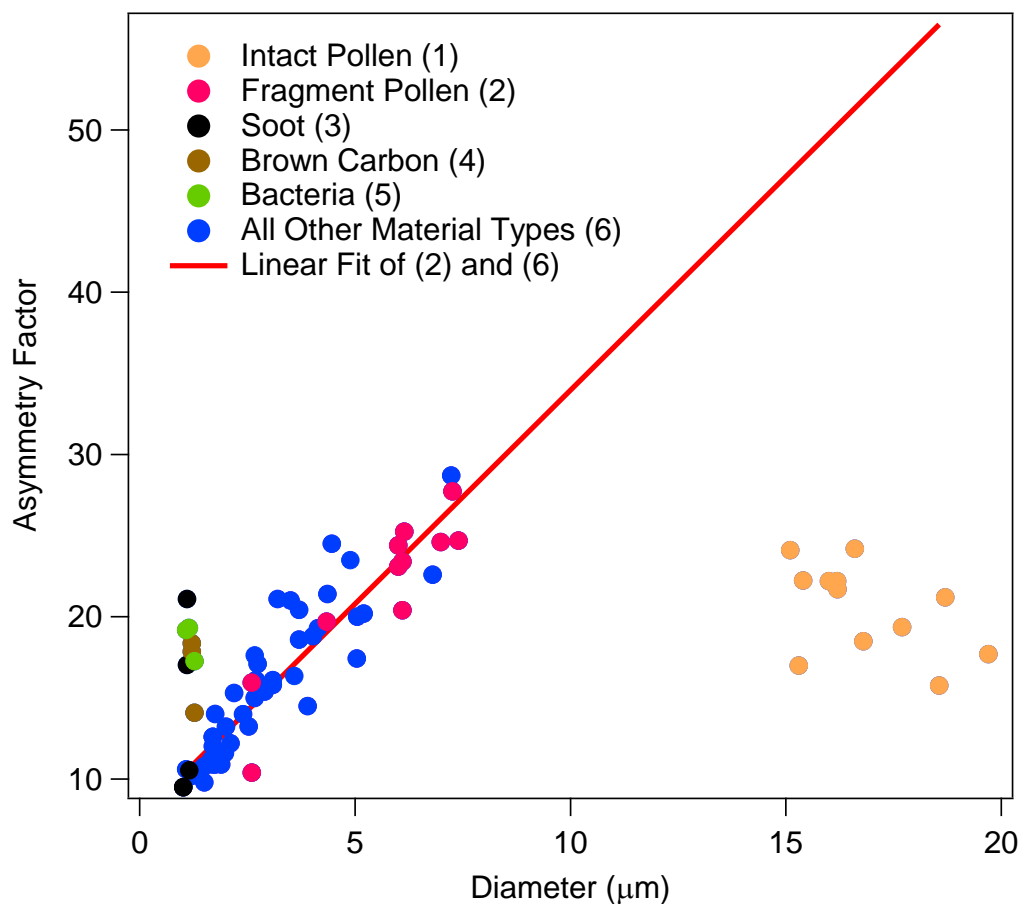


1164

1165 **Figure 6.** Fraction of particle number exhibiting fluorescent in a given channel versus particle
 1166 diameter for various material types for four different thresholds definitions. Data markers shown
 1167 only when disambiguation of traces is necessary. Brown carbon sample denoted by BrC.



1176 **Figure 7.** Stacked particle type size distributions for representative particle classes shown using
 1177 four separate thresholding strategies. NF+ particle type (right-most column) represents particles
 1178 that exceed the FL2 and/or FL3 upper bound of the Wright et al. (2014) FP3 definition and that
 1179 are therefore considered as one set of “non-fluorescent” particles by that definition. Legend
 1180 above top rows indicate threshold definition used.



1181

1182 **Figure 8.** Median values of particle asymmetry factor versus particle size for all particle types
1183 analyzed. Fitted linear regression shown, with equation $y = 2.63x + 7.64$ and $R^2 = 0.87$. Linear
1184 regression analysis was done for samples pooled from the categories of Fragmented Pollen (2)
1185 and All Other Material Types (6).